Characterization of mutations and phenotypes associated with HYAL2 deficiency

By

S M Naimul Hasan

A Thesis submitted to the Faculty of Graduate Studies of

The University of Manitoba

in partial fulfillment of the requirements of the degree of

Master of Science

Department of Biochemistry and Medical Genetics

Faculty of Health Sciences

University of Manitoba

Winnipeg

Abstract

Hyaluronidase 2 (HYAL2) is an endoglycosidase involved in the cleavage of hyaluronic acid (HA). HA is abundantly present in the extracellular matrix (ECM) and reported to have a functional role during embryonic development. Abundant HA has been found in the provisional matrix of the developing skeleton, craniofacial mesenchyme, endocardial cushions and smooth muscles of the gastrointestinal tract of the mouse. Cardiac cushion explant experiments showed that high molecular mass HA promoted epithelial to mesenchymal transition (EMT) while small HA fragments inhibited EMT signaling and induced cellular proliferation. Recently through linkage analysis, followed by next generation sequencing and computational analysis, two separate HYAL2 mutations (K148R and P250L) were identified in Amish and Saudi Arabian families with the syndromic cleft palate. We hypothesize that mutations in *HYAL2* cause deficiency of HYAL2 enzyme and increase HA levels in the craniofacial region. Elevated HA in the craniofacial area interferes with the differentiation of osteoblasts leading to decreased bone development.

Comparison of the phenotypes of patients with HYAL2-mutations to the phenotype of the *Hyal2-/-* mouse from our lab showed similarities including cleft palate (submucosal with underdeveloped viscerocranial bones in mice), heart abnormalities and hearing loss. Functional studies of the mutated forms of HYAL2 expressed in HYAL2-deficient mouse embryonic fibroblasts (MEFs) showed that both mutations destabilized the HYAL2 protein and significantly reduced the HYAL2 level compared to the wild type. Histological analysis of the craniofacial region showed increased HA and reduced condensation of the matrix in the nasopharynx and palate region of HYAL2 deficient compared to wild type mice. Further, assessment of some markers of bone development and differentiation using immunohistochemistry revealed

decreased development of the palatine, vomer and maxillary bones in the HYAL2 deficient mice. Our results indicate that HYAL2 deficiency affects HA turnover during craniofacial development, causing syndromic cleft lip/palate (CLP) and suggesting a possible role for HA in regulating osteoblast differentiation and development.

Dedication

"It doesn't matter which side of the fence you get off on sometimes. What matters most is getting off. You cannot make progress without making decisions."

—Jim Rohn

Dedicated to the memory of my father S M Abdul Bari, who always guided and supported me, whatever decisions I took.

Acknowledgements

At first, I would like to appreciate and thank my supervisor, Dr. Barbara Triggs-Raine, who has guided me to develop every inch of this work. My life in Canada would not be possible without your support. You gave me the strength every time I was falling down. I was blessed with so many sweet memories from the lab and your family which helped me to survive here alone. Your calmness, perseverance, and depth of knowledge always amazed me.

My sincerest gratitude towards my advisory committee members, Dr. Mark Nachtigal and Dr. Sabine Hombach-Klonisch for their valued guidance and suggestions in every committee meetings.

Dr. Biswajit Chowdhury, you were another person not be forgotten in my entire life. Having the support of a histology and imaging "guru" by my side always made things easier. Your continuous willingness to help and the positive outlook for research have broadened my views in pursuing a career in science.

Special thanks to Dr. Richard Hemming, who has taught me to walk confidently in the Triggs-Raine lab. Your experienced technical suggestions have helped to be confidant and troubleshoot experiments. Agnes Fresnoza and Dr. Wafa Kammouni thank you for keeping me cheerful in the very last days of me in the lab. I wish for your well-being and success.

Nazneen Afroz, my loving wife my words will never express the amount of mental support you have provided me. I appreciate and empathize the sufferings you went through during this long distance Canada-Bangladesh life.

Last but not the least, I would like to thank Biochemistry and Medical Genetics department for the continuous support during my study period.

Table of contents

List of figures

List of tables

List of appendices

Appendix 1: List of EMT related genes and their target used in the EMT array experiment.

List of abbreviations

ABC   avidin biotin complex

ABC   ATP binding cassette transporter

Asp   aspartic acid

R   Arg/Arginine

BLAST   basic local alignment search tool

bp   base pair

BSA   bovine serum albumin

CD44   cluster of differentiation antigen 44

CL/P   cleft lip and palate

CP   cleft palate

CPC   cetylpyridinium chloride

DAB   diaminobenzidine

DMAB   p-dimethylaminobenzaldehyde

DMEM   Dulbecco's modified Eagle's medium

DNA   deoxyribonucleic acid

E   embryonic day

ECM   extracellular matrix

ELISA   enzyme linked immunosorbent assay

EMT   epithelial to mesenchymal transition

FNP   frontonasal process

Glu   β-glucuronidase

Glu   glycine

GlcNAc   n-acetyl-glucosamine

GlcUA	glucuronic acid
h	H
HA	HA
HARE	hyaluronan receptor for endocytosis
HAS	hyaluronan synthase
H & E	hematoxylin and eosin
HEK293	human embryonic kidney cells
HMW	high molecular weight
HRP	horse radish peroxidase
HYAL1	hyaluronidase 1
HYAL2	hyaluronidase 2
HYAL3	hyaluronidase 3
HYAL4	hyaluronidase 4
Hyal5	hyaluronidase 5-encoding gene
HYALP1	hyaluronidase pseudogene 1
K	Lys/lysine
KO	knockout
L	Leu/leucine
LB	Luria broth
LBA	Luria broth with ampicillin
LMW	low molecular weight
LNP	lateral nasal prominence
LYVE-1	lymphatic vessel endothelial receptor 1

MAND	mandibular prominence
MES	medial epithelial seam
MEFs	mouse embryonic fibroblast
mg	milligram
min	minutes
mm	millimeter
MNP	medial nasal prominence
MMW	Medium molecular weight
MPS	mucopolysaccharidosis
MxP	maxillary prominence
NCBI	National Centre for Biological Information
NCC	neural crest cells
ng	nanogram
NGS	next generation sequencing
nm	nanometers
ONPG	ortho-nitrophenyl-β-galactopyranoside
OSX	osterix
P	Pro/proline
PBS	phosphate buffered saline
PCR	polymerase chain reaction
PDB	protein data bank
PG	proteoglycan
PH20	sperm surface protein 20

PyMol   python enhanced molecular graphics tool

R   arginine

S   second (s)

SDS   sodium dodecyl sulfate

SDS-PAGE   SDS-polyacrylamide gel electrophoresis

SOC   super optimal broth with catabolite repression

SPAM1   sperm adhesion molecule 1

TEMED   tetramethylethylenediamine

TBST   tris-buffered saline with 1% Tween-20

U   unit

Hex   β-N-acetylhexosaminidase

μF   micro farad

μg   microgram

μl   microliter

WT   wild-type

Chapter 1: Introduction

1.1 Hyaluronic acid and hyaluronidase

The hyaluronidase enzyme was discovered in 1928 and has since been described to have catalytic activity against the glycosaminoglycan hyaluronic acid (HA), a repeating polymer of glucuronic acid (GlcUA) and β-N-acetylglucosamine (GlcNAc)[1]. These enzymes have also been reported to be weakly active against two other glycosaminoglycans (GAGs), chondroitin and chondroitin sulfate. Duran-Reynals first reported hyaluronidases as "spreading factors" present in the human testes, and other tissues, that assist in the diffusion of subcutaneously injected substances[2–4]. Hyaluronidases are members of the glycosidase family 56 group of hydrolases[5]. They are endoglycosidases that randomly hydrolyze β-1,4 linkages between GlcNAc and GlcUA residues of HA. Based on mechanisms of enzymatic catalysis, hyaluronidases were grouped into three classes: mammalian hyaluronidases (EC 3.2.1.35), leech hyaluronidase (EC 3.2.1.36) and microbial hyaluronidases (EC 4.2.2.1). The first two classes of mammalian and leech hyaluronidases degrade HA by hydrolyzing the glycosidic bond whereas the microbial hyaluronidases degrade HA by a β-elimination reaction to form a double bond in the product.

1.2 Mammalian hyaluronidases

In humans, hyaluronidase-related genes are found as a cluster of two groups of three. On chromosome 3p21.3, three hyaluronidase-related genes, *HYAL1*, *HYAL2,* and *HYAL3* have been localized, and an additional cluster of three genes, *HYAL4*, *HYALP1* and *PH20/SPAM1* are found on chromosome 7q31.3[6]. *HYALP1* is not translated into a protein product because of an internal stop codon. The remaining five human hyaluronidase-related sequences have 33 to 42% identity in their amino acid sequences, which suggests a gene duplication event that formed a cluster of three genes that was subsequently duplicated on a second chromosome[5].

In mouse, the orthologous hyaluronidase genes are clustered in two groups of three on chromosome 9 (*Hyal2*, *Hyal1*, *Hyal3*) and chromosome 6 A2 (*Hyal4*, *Spam1,* and *Hyalp1*), respectively. The numbering of these genes is a product of genetic studies that identified several candidate lung cancer tumor suppressor genes in humans, including *LuCa2*, *LuCa1,* and *LuCa3* which were later identified as hyaluronidases[7,8]. Apart from these six hyaluronidase-like genes another orthologous hyaluronidase gene, *Hyal5,* is found on mouse chromosome 6[9].

1.3 Distribution of mammalian hyaluronidases

Gene expression studies showed that only the human and mouse genes encoding HYAL2, HYAL1, and HYAL3 are broadly expressed in somatic tissues. The HYAL4-encoding gene is primarily expressed in placenta[6] and expression of the SPAM1-encoding gene is restricted to the male reproductive tract[10.] HYAL4 is thought to be a chondroitinase[11,] and no activity has been associated with HYAL3[12.] This leaves only HYAL1 and HYAL2 which are thought to play a significant role in HA degradation in somatic tissues.

1.3.1 Activity of mammalian hyaluronidases

Most biochemical characterization of the hyaluronidases has been done on HYAL1 because it was the first to be isolated and was readily assayed. Although HYAL1 was present at a very low concentration in human serum, it showed high specific activity[8]. HYAL1 had an acid pH optimum and could degrade HA of all sizes[13]. Several assays have been developed to determine the activity of hyaluronidases including the Reissig assay[14], a microtiter-based ELISA (Enzyme-Linked Immunosorbent Assay)[15], and HA-substrate gel zymography. In HA-substrate gel

zymography, a native gel is prepared containing HA and hyaluronidase activity is measured semi-quantitatively by analyzing the size and completeness of the clearing of the gel[16]. Measuring HYAL2 activity using these approaches has been challenging. Several studies failed to show activity for HYAL2, possibly because of weak activity or a requirement for other cellular partners for its activity[17–21]. Differences in the localization of HYAL2 and optimal pH for its activity by research groups have further complicated its study. For example, the optimum pH for HYAL2 activity has been reported as both acidic and near neutral [20,21], possibly reflecting differences in the structure of the enzyme or possibly the presence of contaminating HYAL1. The model proposed for HA degradation suggested HYAL2 requires a Na^+/H^+ exchanger NHE1 for the acidification of its local environment and this exchanger could be one of the additional components HYAL2 needs for its activity[18]. Moreover, some other studies also reported HYAL2 and HYAL1 activity required concomitant expression of the cell surface receptor CD44 (cluster of differentiation antigen 44)[21], possibly another important candidate required for the quantification of activity. Characteristics of the substrate HA also differs between HYAL1 and HYAL2. While HYAL1 appears to be active against the lysosomal pool of HA, HYAL2 appears to be actives towards extracellular HA. Considering the nature of HYAL2's function, additional studies are needed to develop a robust assay for measurement of its activity.

1.3.2 Hyaluronidase 1 (HYAL1)

The *HYAL1*/*Hyal1* gene is comprised of 7 exons which encode several alternatively spliced mRNA species that can be translated into a 435 amino acid protein[8]. HYAL1 is an acid-active enzyme that cleaves HA to tetrasaccharides by hydrolyzing the β1-4 glycosidic bond between GlcUA and GlcNAc[8]. Almost all human tissues express *HYAL1* mRNA, but it is most highly

expressed in tissues where HA degradation is highest like the liver, kidney, spleen, and bone marrow[22].

Studies of HYAL1 from murine macrophage showed that it is synthesized as a 52 kDa protein that is primarily secreted out of the cell and re-internalized by endocytosis where it undergoes proteolytic cleavage and transforms into 48 kDa mature protein[23]. Further analysis suggested that serum HYAL1 gets endocytosed by liver sinusoidal cells.[24] Studies from HEK 293 (Human Embryonic Kidney 293) cells suggested HYAL1 function depends on the presence of the CD44 receptor, supporting previous studies showing the requirement for a receptor for HA internalization to the lysosome[21]. The crystal structure of HYAL1 showed it was an alpha/beta barrel containing the active site resides at the center of the barrel[25]. Structure/function studies have indicated that residues identified to be critical for catalysis in the bee venom hyaluronidase are conserved in HYAL1[13].

HYAL1 deficiency causes abundant HA accumulation in the lysosomes of macrophage and fibroblasts of joint tissues, resulting in mucopolysaccharidosis (MPS) IX, which is primarily characterized by an arthritis-like phenotype involving multiple joints[26]. A mouse model of HYAL1 deficiency also exhibited a similar phenotype, with pathology limited to the joints[27].

1.3.3 Hyaluronidase 2 (HYAL2)

The *HYAL2/Hyal2* genes are composed of six exons which encode a 1.9 kbp mRNA that can be translated into a 473 amino acid protein[22,28]. It is predicted to have a 20 amino acid signal sequence that directs the protein to the endoplasmic reticulum where it is modified by glycosylation and addition of a glycosylphosphatidylinositol (GPI) anchor[29]. The GPI anchor

aids in HYAL2's association with lipid rafts at the cell surface[30]. The fully processed protein has a molecular mass of approximately 60 kDa in mouse tissues[17].

Ubiquitous expression of *HYAL2*/*Hyal2* mRNA was reported in expression studies from adult and embryonic human[28] and mouse[31] tissues. Histologically, HYAL2 was found to be detectable, but at variable levels in the endothelial cells of most mouse tissues, and in specialized epithelial cells of the lung, kidney, brain, intestine, and oviduct[32].

Localization of HYAL2 has been controversial[33]. The first study of HYAL2 localized it in the lysosome by following the expression of a HYAL2 fusion with green fluorescent protein (GFP)[17]. In this experiment, the GFP-tag was attached to the C-terminus which was later found to prevent the addition of the GPI anchor to HYAL2, or lead to cleavage of the GFP-tag. Whatever the case, normal sorting of HYAL2 after processing did not occur and subsequent studies by this group[34] and others[29,35], clearly indicated the presence of HYAL2 at the cell surface. Moreover, the characteristics of a GPI anchored protein support its localization to the cell surface rather than in the lysosome. However, in some cell types, HYAL2 appeared to have an intracellular localization[36]. Later, different studies suggested HYAL2 localized to the cell surface[37], mitochondria[38] and nucleus[39] leaving the localization of HYAL2 unclear. The most recent studies of endogenous mouse HYAL2 from our own laboratory, and using control tissues from HYAL2 deficient mice, indicate that HYAL2 is expressed on the surface of many cells, but can be found intracellularly in some cell types[32].

Studies of HYAL2 activity have also been controversial. The earliest studies suggested HYAL2 functioned as a weakly active hyaluronidase that had specificity towards high molecular mass HA, and activity at both neutral and acidic pH[17]. However, subsequent studies did not detect activity for HYAL2 at either acidic or neutral pH[29]. A Na^+-H^+ exchanger was proposed to

maintain the acidic environment required for the activity of HYAL2[18]. Platelet HYAL2 appeared to be active when it is translocated from α-granules to the platelet surface.[40] Convincing evidence that HYAL2 played a role in HA metabolism came from expression of HYAL2 in HEK293 cells where there was increased turnover of HA, however in this case the activity was found to require the presence of the HA receptor, CD44[21].

1.3.4 Mouse model of HYAL2 deficiency

The inability to definitively demonstrate HYAL2's activity made the generation of a mouse model deficient in HYAL2 an important step to understanding its role in HA catabolism and maintaining ECM (Extracellular Matrix) homeostasis. An initial attempt to generate a HYAL2-deficient mouse was unsuccessful, presumably due to embryonic lethality[34]. Later, a HYAL2 KO mouse was successfully generated from our group with collaborators and characterized[41]. An outbred background (129/Ola/CD1/C57BL/6) was used for the initial generation of the HYAL2 KO mouse, which were backcrossed for 6 generations on the C57BL/6 background. The initial characterization revealed elevated serum HA, but only minor hematological and skeletal abnormalities, including an increased interorbital space and a shortened snout. There was also some evidence of reduced survival[41]. Subsequent characterization of the HYAL2 KO mouse on the outbred background showed heart abnormalities in surviving HYAL2 KO mice that was characterized by expansion of the atrium and valves[42]. Ultrasound studies revealed the presence in 40% of surviving animals of cor triatriatum sinister (three atria)[43]. Beyond the craniofacial and heart abnormalities, comparison with subsequently identified human patients revealed that 1/3 of HYAL2 KO mice died postnatally but before day 7 of age. These mice had evidence of submucosal cleft palate and poor mineralization of the central facial bones, as well as hearing

loss[44]. Accumulation of HA was evident in most tissues of the HYAL2 KO mice, suggesting an important role for HYAL2 in the removal of extracellular HA[32].

1.4 Hyaluronic acid

1.4.1 Structure and distribution

In 1934 Karl Meyer identified HA as a component of the vitreous humor[45]. The term hyaluronic acid was derived from the Greek word 'hyalos' meaning glass, and uronic acid. HA was mostly found in the ECM as a repeating unit of GlcNAc and GlcUA disaccharides linked by β1-3 and β1-4 glycosidic bonds. Endrez Balazs coined "hyaluronan" to represent both the free acids and salt conjugated forms of HA[46]. HA ranged in size from short oligosaccharides to low molecular weight (LMW) and high molecular weight (HMW) with more than 10^5 saccharide units[47]. The definition of these sizes differs among papers and has not been standardized in the literature. The GlcUA component of the HA provided it with anionic properties which are speculated to make HA a continuous network in the shape of a random coil by attracting water molecules[48]. Unlike other GAGs, HA was non-sulfated and was not attached to a core protein[49].

HA was detected in almost all vertebrate tissues and reached its highest concentration in the umbilical cord, synovial fluid, skin, and vitreous body of the eye. In addition to this, HA was found in striated, skeletal, and rectus muscles of the adult rat as well as almost all organs in mouse and rat[42,50]. Study of the HA distribution in rat reported that skin contained almost half of the HA present in the body, another 25% of HA was found in the skeleton and joints, and the remainder was equally distributed in the muscle and viscera[51]. In humans, the highest concentration of HA was found in the umbilical cord (4.1mg/g), synovial fluid (91.4 mg/g), skin (0.2 mg/g) and vitreous body (0.14 mg/g)[52]. High levels of HA were also present in the visceral

organs and in the developing embryo[53]. These studies suggested the HA level is higher during vertebrate development[53] and it plays an important role in maintaining normal physiology. Localization studies suggested HA is primarily present in the extracellular space and pericellular coat of cells, although it is also sometimes found intracellularly[54].

1.4.2 Synthesis and turnover

Unlike other GAGs which are synthesized in the endoplasmic reticulum and Golgi apparatus, HA synthesis occurs in the plasma membrane[55]. HA is synthesized by the HA synthases (HASs) which are glycosyltransferases embedded in the plasma membrane. HAS polymerizes nucleotide sugars, GlcUA and GlcNAc sequentially to the reducing end of the growing HA molecule[56]. HA is also unique compared to the other GAGs because it lacks a protein backbone, and thus only the presence of nucleotide sugars is required to synthesize a new HA chain. The mechanism of HA transport across the cell membrane is currently unclear as reports from bacteria and HEK293 cells suggested HA was exported out of the cell by an ATP-binding cassette (ABC) transporter[57,58]. Recently, a pendulum model speculating simultaneous synthesis, assembly and transport of HA by the HAS alone was put forward[59].

1.4.3 Mammalian HA synthases

In mammals, three HASs, HAS1, HAS2 and HAS3 are encoded by genes mapped on three different chromosomes. The three isoforms of HAS are very similar, but they produce HA of different sizes and at different rates[60]. Although HAS1 and HAS2 produce HMW-HA ranging from 2×10^5 to 2×10^6 Da, HAS2 is catalytically more active than HAS1. HAS3 appears to have the highest rate of synthesis but produces HA that is smaller in size (~1×10^5 Da). Variation in the

sizes of HA may be required to regulate the diverse biological roles within an organism. The three HAS enzymes are expressed throughout the mammalian lifespan, but HAS2 was broadly expressed during early development while HAS3 expression was more evident in adult tissues[61]. The differences in *HAS* expression at different stages in various tissues suggested an important role during mammalian development, and subsequent knockout studies of different HA synthases showed the importance of these genes in normal physiology and disease development[62–64].

HAS1 expression in mice is highest during early gastrulation[65], and initial studies from targeted disruption of *Has1* appeared to be normal[66]. Later studies focusing on brain function reported a deficiency of HAS1 to be associated with increasing epileptic seizures[67]. Although alterations in the mRNA and mutations in *HAS1* have been found to be associated with multiple myeloma, Waldenstrom' syndrome and B cell malignancies, the relationship between the phenotypes and role of HAS1 remain unknown[68,69].

Among the three HAS enzymes, HAS2 is recognized as a major contributor to HA synthesis during embryogenesis[70]. HAS2 deficiency in the mouse is embryonic lethal at E (embryonic day) 9.5 due to the failure of endocardial cushion development and epithelial to mesenchymal transition (EMT) for valve and septa formation[62,71]. This defect was shown to be corrected by the addition of exogenous HA in *ex vivo* explant cultures of cardiac cushions from *Has2* KO embryos[71]. This suggested that HA regulated a cellular signal(s) to control development during embryogenesis. Studies aiming to determine if HAS2 is involved in other abnormalities included a tissue-specific inactivation of *Has2* in the mouse skeleton and suggested that HA is also an essential component for limb development[72]. Given the high level of HA distribution during development, it is important to determine the role of *Has2* and its function in other tissues as well[61].

Although HAS3 is the most active of the HASs, its expression was found only in ectoderm-derived organs[65]. Studies from HAS3 KO[63] as well as HAS1/HAS3 double KO[64] mice showed no differences

in phenotype other than showing more resistance to ventilator-induced lung injury and accelerated wound closure. More detailed studies, however, showed reduced HA in the brain accompanied by reduced extracellular space and crowding of the neurons which was associated with predisposition to seizures in the brain-specific *Has3* KO mouse[67].
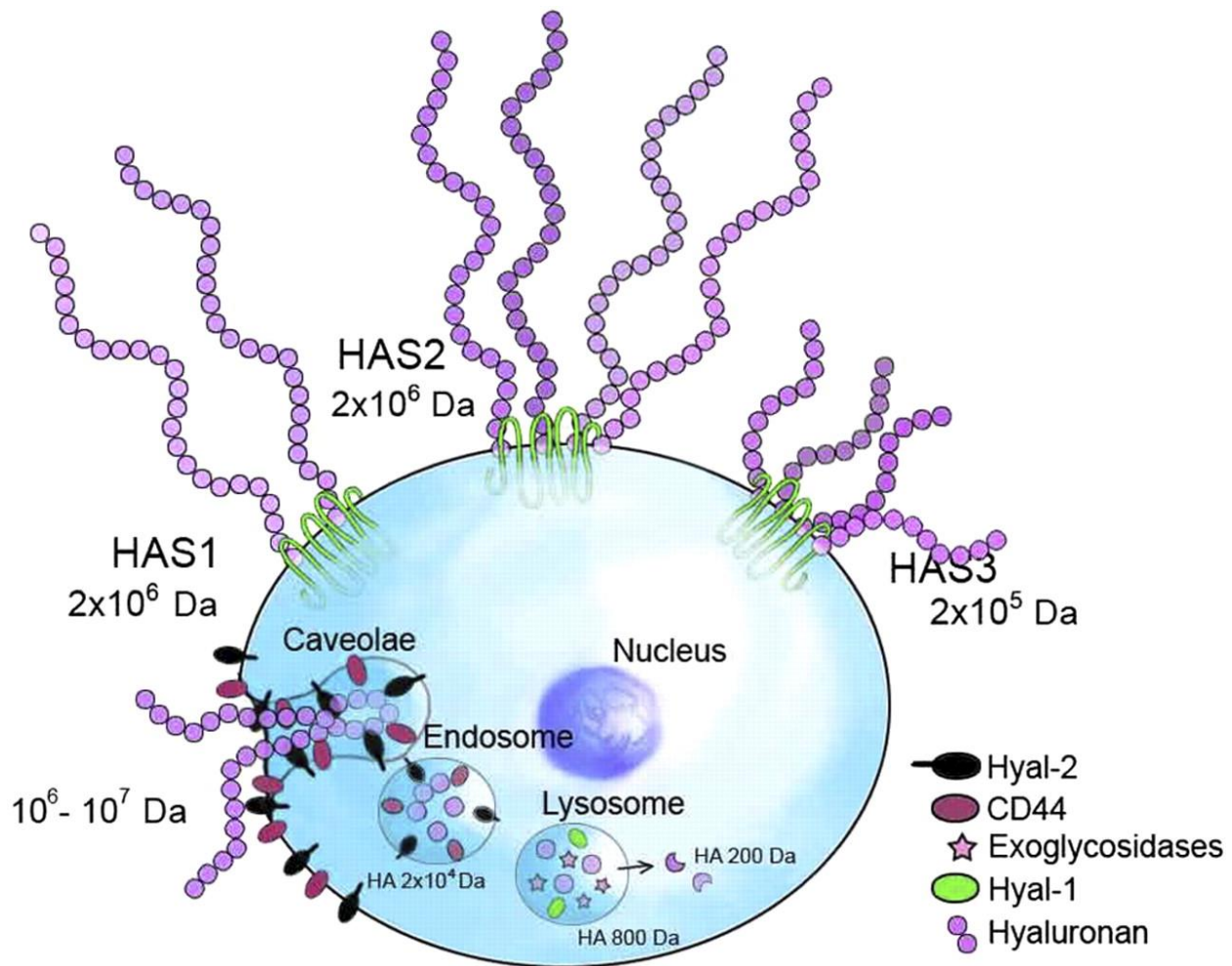
Figure 1. 1 Regulation of HA size and rate of synthesis by HAS.

The three HAS proteins produce differing amounts and sizes (chain lengths) of HA. This figure shows that HAS1 synthesizes small amounts of HMM-HA (2×10^6), HAS2 produces significantly more HMM-HA (2×10^6) and HAS3 is the most active of the HAS enzymes but produces LMW-HA(2×10^5). HYAL2 degrades HA bound with receptors like CD44 and degrades HMW-HA into MMM-HA. The MMM-HA are transported into lysosomes for further degradation facilitated by HYAL1 and exoglycosidases. HA degradation is described in more detail in the following sections. (Reproduced from Sara Stridh et al. Am J Physiol Regul Integr Comp Physiol 2012;302: R1235-R1249i)

1.4.4 HA turnover

HA turnover is extremely high among the ECM molecules[73,74]. It is estimated that the daily turnover rate of HA is about one third or 5 of the 15 g of HA normally present in an average adult person[75]. Although the initial half-life of HA was estimated at 2-4 days, this half-life is tissue dependent. For instance, the HA turnover rate is 2-5 min in the blood, 1-2 days in the skin, and much slower in the cartilage at about 2-3 weeks[76,77]. Almost 30% of HA degradation is localized to the tissues of origin[52] and of the remaining 70%, most is removed by the endothelial cells of the lymphatic system[78] , leaving only 10% that is eliminated from the blood by the liver[76], kidney and spleen[79]. HA mass gets reduced from that in the local tissues (10^5 or 10^6 Da) when it transits the lymphatic system, suggesting the involvement of HYAL2. Only 1% of the HA excreted from the blood is removed in the urine with a low molecular mass (>12000 Da)[78].

1.4.5 HA degradation

Complete degradation of HA to monosaccharides required the catalytic functions of both the endoglycosidase- hyaluronidase, and the exoglycosidases β-N-acetyl-D-hexosaminidase and β-D-glucuronidase[80]. The HA polymer first gets hydrolyzed at the β1-4 linkage formed between the GlcUA and GlcNAc. The resulting fragments act as a substrate for the β-D-glucuronidase, revealing GlcNAc, which in the substrate for β-N-acetyl-D-hexosaminidase[81]. A model was proposed for HA catabolism suggesting cell surface receptors like CD44, LYVE-1 (Lymphatic Vessel Endothelial Receptor 1), and HARE (HA Receptor for Endocytosis) bind with HMM-HA and cleavage by HYAL2 promotes endocytosis of the resulting fragments into the lysosome. Inside the acidic environment of the lysosome, the acid active HYAL1 degrades the HMM-HA to smaller fragments which in later stages get degraded by the exoglycosidases, β-

hexosaminidase (Hex) and β-glucuronidase (Glu). Although the role of HYAL3 in HA degradation is not clear yet, overexpression studies showed that it increased HYAL1 activity, suggesting a role in HA degradation[12].
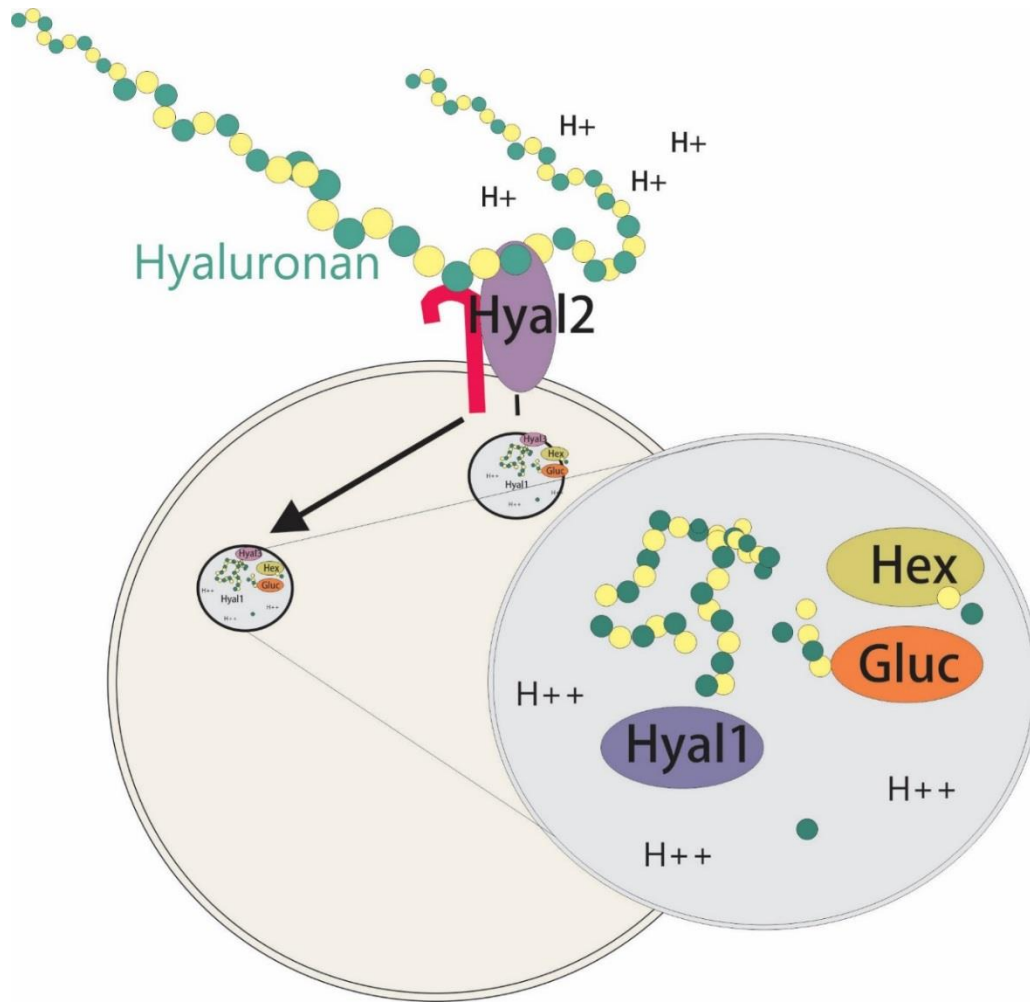
Figure 1. 2 Proposed Model for HA degradation

Degradation of HA into different sizes occurs by HYALs. This can be achieved by 1) HYAL2 on the plasma membrane which hydrolyzes HMW-HA to MMW-HA. HA remains attached with the cell or matrix associated receptors like CD44, HARE, or LYVE have been proposed to assist HYAL2 in HA degradation. 2) Later, the resulting MMW-HA fragments are internalized by receptor-mediated endocytosis and transported into the lysosome. 3) Finally, within lysosome, the acid active HYAL1 cleaves MMW-HA into HA oligosaccharides making them as available for breakdown into sugar units achieved by the exoglycosidases, Glu and Hex. Cells uptake the single sugar units and reuse for new molecule synthesis. (Figure courtesy of Dr. Barb Triggs-Raine)

1.4.6 HA distribution during development

Studies showing HA distribution during early development suggested HA levels rapidly decreased upon implantation of the blastocyst onto the uterine wall but increased later during the appearance of the primitive ectoderm and endoderm[82,83]. Mapping of HA distribution during mouse embryogenesis demonstrated that by E11.5 - E13, there was abundant HA present in the craniofacial mesenchyme, endocardial cushions, axial skeleton, smooth muscle of the gastrointestinal tract and connective tissue throughout the body[82].

1.4.7 HA function during development

HA has been demonstrated to be a critical component during vertebrate development and reported to play a role during tissue/organ morphogenesis by influencing several molecular functions. HA was shown to regulate embryonic cell behavior by creating a hydrated low-resistance matrix which provided cells mechanical support and gave contact inhibition characteristics that stimulated cell proliferation and migration[84]. HA has been reported to modulate the hydration of the environment by forming an HA-dependent pericellular matrix during mitosis that promoted partial separation and rounding of the ongoing dividing cells[54]. Apart from providing mechanical support to the ECM that contributed to maintaining tissue homeostasis, HA also acted as a key component to assemble the ECM by interacting with the proteoglycans (PGs) through link modules, cell surface receptors and possibly through interactions with HA synthases[85,86]. HA also served as a binding partner for other proteins and provided ligands for cell attachment and motility which might shape embryonic development[87–89]. In the developing matrix, HA influenced the level of intercellular signals affecting cell growth and differentiation by interacting with growth factors[90]. Moreover, HA interactions with its

receptors changed the ECM properties and regulated different cell signaling events during developmental and pathologic conditions; this is influenced by HA size and abundance.

1.4.8 HA in EMT

Several avenues of study have shown a role for HA in the regulation of EMT. EMT is a multi-step-process which involves a series of biochemical changes in the epithelial cells as they transform into mesenchymal cells. This change is characterized by a loss of the intercellular adhesion complex, promoting the tightly linked epithelium to become motile mesenchyme. The transformed cells have increased invasiveness as well as migratory and proliferative capacity[91]. The composition and state of the pericellular matrix microenvironment are very important in determining the state of the cells. Elevated secretion of EMT components including HA has been reported in cells undergoing EMT[92].

HA accumulation and degradation play a role in EMT, particularly in the early stages of embryogenesis, where it is critical for tissue formation through the differentiation of the embryonic stem cells to mesenchymal stem cells[93]. Elevated HA in normal epithelial cells has been shown to influence anchorage-independent growth and change the characteristics of the cytoskeletal proteins between cell boundaries[92,94]. Studies of the influence of HAS3 and HAS2 overexpression in human pancreatic cells showed decreased E-cadherin but increased β-catenin which promotes EMT in cells. After completion of the transition, vimentin is upregulated in mesenchymal cells[92,95].

Earlier reports have shown increases in HA levels during several embryonic EMT processes including cardiac cushion formation[96], palatal shelf fusion[97], and neural crest transition[98]. Strong evidence to support a role for HA in EMT came from the *Has2* KO mouse, where reduced HA in

the endocardial cushions of E9.5 embryos prevented the endothelial cells lining the cushion from being converted into mesenchyme due to the defective HA-induced ErbB2/3 and Ras signaling[62,71]. Endocytic removal of HA and its associated PGs is also a critical step during this process[99]. Mice defective in the degradation of the HA-binding PG versican showed abnormalities in organ development and closure of the secondary palate[100]. *In vitro* studies using blocking antibodies against CD44, a cell surface receptor of HA also affected the properties of the ECM in development[101,102]. During development, mesenchymal cells undergo condensation prior to differentiation and CD44 is often localized to the condensation sites which play a role in many epithelial-mesenchymal interactions. Removal of HA during the condensation process changes the ECM characteristics of the mesenchyme leaving the residual HA to crosslink with the cell surface receptors of the adjacent cells and promote differentiation[103,104]. For example, during embryonic skin and bone development, mesodermal condensation results due to the removal of the intercellular HA by CD44 mediated endocytosis and continues the differentiation to form hair follicles and chondrocytes[3,105]. Any conditions altering the interaction of HA with its receptor or affecting the removal of it might interfere with normal development resulting in cardiac[106] or craniofacial abnormalities, which involves one-third of all congenital birth defects in humans[107,108]. HA is also reported to act as a critical component of the microenvironment of hematopoietic stem cells (HSC) and plays a role in stem cell proliferation, migration, and differentiation[109]. HSC maturation occurs after degradation of the HA that arrests HSC proliferation[110].

1.4.9 HA in craniofacial development

During development, cranial neural crest cells (NCC) -a multipotent cell population originating from the neural crest- migrate and differentiate to establish the basis of the future facial structure. EMT is required for the migration, proliferation, and differentiation of the NCC during craniofacial development. The palate shelf forms initially by vertical outgrowths around both sides of the tongue which in subsequent stages orients itself above the dorsum of the tongue by horizontal movement coordinated by a cellular migration process known as palatal shelf elevation. HA synthesis has been documented to be altered during EMT[62] and migration[54]. In addition, during palatal shelf elevation increased HA is thought to provide a hydration force as part of the ECM[111]. Histochemical and biochemical studies during palate shelf elevation showed abundant HA in the growing ECM which decreased after the completion of elevation[112,113]. Experiments from *Xenopu*s showed the HA-rich ECM promoted NCC migration and differentiation into chondrocytes during craniofacial development[114].

1.5 Mammalian craniofacial development

Formation of the cranial NCC is the first and critical step for craniofacial development[115]. The NCC cell is an evolutionary conserved vertebrate cell type that is able to differentiate into several craniofacial tissues. During embryogenesis, NCC cells arrive from the dorsal aspect of the neural tube, particularly from the borders between the developing neural fold and non-neural ectoderm, and subsequently, migrate to populate the FNP (frontonasal process) and pharyngeal arches[116]. A tightly regulated signaling network coordinates the migration of the NCC to support normal craniofacial morphogenesis[117]. While the FNP arises from the most anterior NCCs, derived from the fore-brain and mid-brain regions, the maxillary and mandibular prominences in

the first pharyngeal arch gets populated by the NCC of the posterior mid-brain and rostral hind-brain regions[118]. After migrating to the FNP, NCCs undergo rapid cell proliferation to support the rapid growth of the facial prominences. For the proper development of the craniofacial structures, NCC interactions with the surrounding forebrain and facial ectoderm are crucial[119]. After differentiation of the NCC the FNP forms the forehead, middle of the nose, upper lip, philtrum and primary palate[120]. The side of the nostril and top of the nose appears after the fusion of the lateral FNP with the LNP (lateral nasal prominences) and medial region of the maxillary prominences. The expansion and cleavage of the first pharyngeal arch forms the maxillary (MxP) and mandibular prominences (MAND) which later form the upper and lower jaw respectively[120]. Alterations in any component of this multistep process that regulates the cranial NCC migration, proliferation and differentiation during developmental stages can result in craniofacial abnormalities. Orofacial clefting characterized by the separation of the lip or the palate or both is one of the most common craniofacial abnormalities and affects almost 3% of live births[121]. Some other types of craniofacial abnormalities include but not limited to, craniosynostosis, characterized by premature closure of the calvarial suture which affects the shape of the skull and facial symmetry, and hemifacial microsomia also known as Goldenhar syndrome where there is underdeveloped tissue appearing as sidedness of the facial tissues.

1.5.1 Primary palate development

The development of the primary palate takes place after the FNP has developed into the MNP and LNP. In early embryonic stages extensive cellular growth initially allows the MxP to come into contact with the LNP and subsequently with the merged MNP. The freely projecting MNP and LNP initially fuses together and later the MxP and MNP comes closer pinching two layers of

surface epithelium between them which eventually will form the future nasal and oral epithelium (Fig. 1.3 A, E10.5). In subsequent developing stages, the two layers of the epithelium disintegrate forming a continuous mesenchyme between the MNP and MxP which acts as the core of the primary palate. Failure in the fusion of the MxP and the FNP results in cleft lip[120].

1.5.2 Secondary palate development

The development of the secondary palate is independent of the lip and primary palate. In the mouse, at E11.5, (corresponding to the 6th week of human gestation) the maxillary process- primer of the palate shelf outgrowth grows vertically down the side of the developing tongue between the stages E12.0 and E13.0. As the jaw develops, the tongue lowers, and the palatal shelves begin to elevate to the horizontal position above the developing tongue at E14.0 (Fig.1.3). The palate shelves then continue to grow horizontally, and the epithelia opposing the palate shelves adhere together in the mid-anterior region and form a transient medial epithelial seam (MES). At E15.5 the palate shelf fuses by the disintegration of the seam and the mesenchyme become confluent to form an intact secondary palate. Eventually, the fusion of the secondary palate will take place anteriorly with the primary palate, resulting in the intact roof of the oral cavity[122]
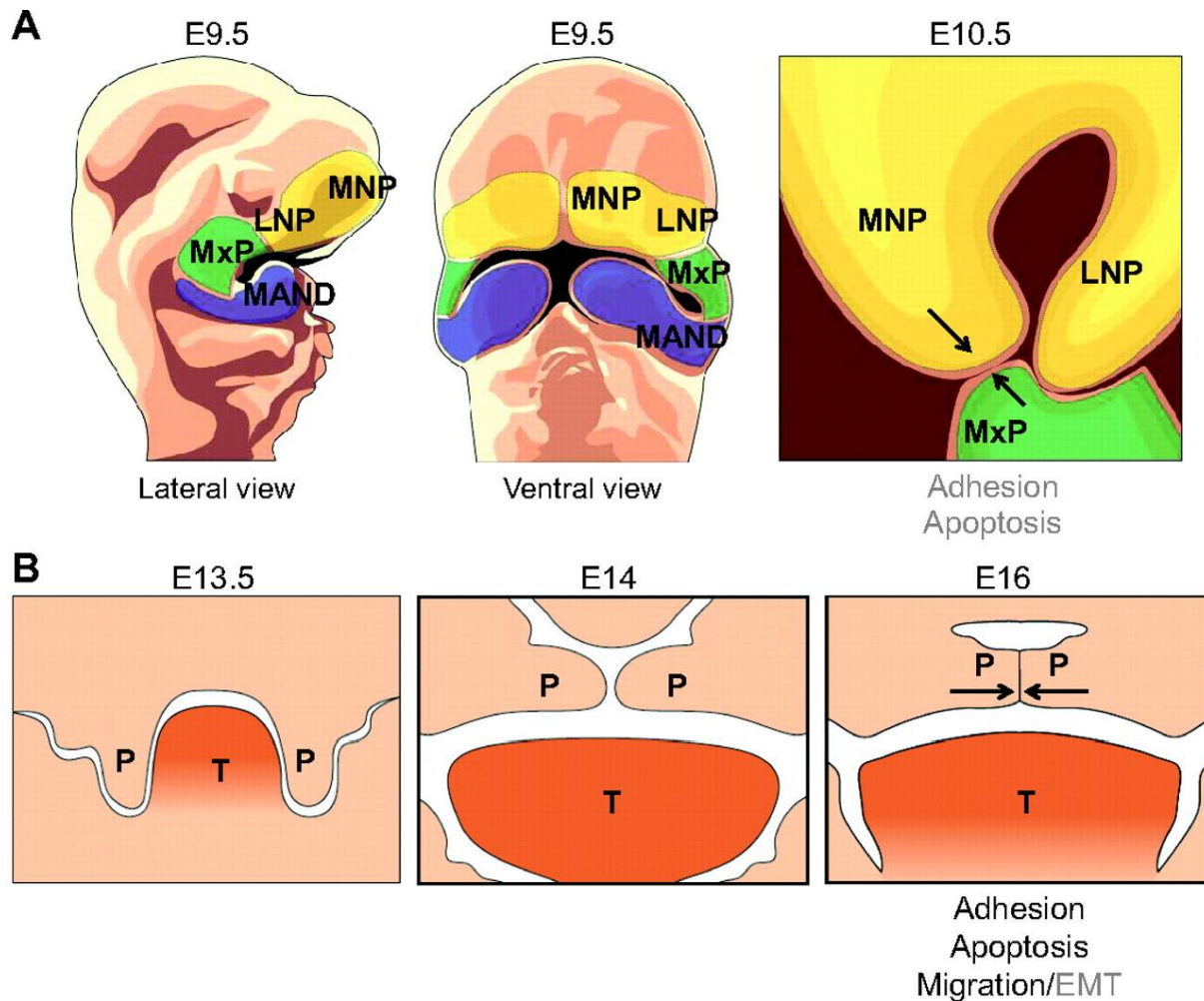
Figure 1. 3 Tissue fusion during craniofacial development. (A) Fusion during murine primary palate development. At E9.5, the FNP (frontonasal process; yellow) starts to develop into MNP (median nasal process) and LNP (lateral nasal prominences). The MxP (maxillary prominence; green) and the MAND (mandibular prominence; purple) also appear at this stage. Around E10.5, tissues between the MNP and the MxP (area between arrows) fuse, followed by fusion of the MNP and LNP. (B) Fusion during murine secondary palate development. At E13.5, the palatal shelves (P) orient vertically along the tongue (T) which at E14, comes towards a horizontal position above the tongue. From E14.5 to E16, opposing palatal shelves fuse (area between arrows) to generate the secondary palate. (Reproduced with permission from Heather J. Ray, and Lee Niswander Development 2012; 139:1701-1711)

1.5.3 Orofacial clefting-abnormalities in palate development

In mammals, separation of the oral cavity from the nasal cavity involves the anterior bony hard palate and the posterior soft palate. Orofacial clefting is one of the most common congenital abnormalities in man, and arises due to disturbances in the fusion of the lips and/or palate during embryonic development. Oral clefts compromise infant's feeding, hearing, speech and psychological development. Although surgical solutions are available, significant long-term health implications remain for the affected individual[123,124]. Orofacial clefting can be classified into two subclasses depending on whether the cleft in the palate co-occurs with cleft lip (CL/P) or involves cleft palate (CP) alone. Further classification of the orofacial clefting was done as: syndromic and non-syndromic orofacial clefting depending on the association of other factors with CL/P. About 70% of CL/P cases were grouped into non-syndromic, while the rest reported to have association of some other human syndromes.[123]. Etiologically it was found that CL/P occurs in males almost twice as frequently as in females, but no direct association of sex linkages have been evident until recently[125].

1.5.4 Genes associated with secondary palate development

The process of lip and palate formation during embryonic development involves the mesenchymal cell proliferation, epithelial adhesion of the initially formed primordia for the fusion of the palate and programmed cell death at the region of the integration. It is likely that a cluster of genes and signaling pathways are involved in the coordination of the cellular transformation process during palate development. This process is universal and failure to achieve any of this phenomenon during development might cause CL/P.

A search of the Online Mendelian Inheritance in Man database (accessed on November 19, 2017) using the term 'non-syndromic clefts yielded more about 1800 entries and a search using syndromic clefts yielded more than 7500 entries[126].

Through positional cloning, clefts in the secondary palate have been reported as an X-linked condition in humans caused by mutations in *TBX22*. The affected individuals had submucosal cleft palate with underdeveloped viscerocranial bones and a thickened connection between the tongue and the base of the oral cavity (ankyloglossia)[127]. Mutation in the *IRF6* (*Interferon regulatory factor 6*)has been linked with Van der Woude's syndrome know as one of the most common forms of syndromic CL/P[128]. Van der Woude's syndrome is autosomal dominant, where patients have a few minor defects, such as lip pits and hypodontia, in addition to CL/P. Mutations in the *P63* gene, which encodes a member of the *P53* family of transcription factors, causes another autosomal dominant form of syndromic CL/P[129]. Different mutations in the multiple domains of the *P63* gene have also been identified in a spectrum of syndromes: ectrodactyly, ectodermal dysplasia and CL/P, Hay-Wells syndrome or Ankyloblepheron ectodermal dysplasia and CL/P, and acro-dermato-ungual-lacrimal-tooth syndrome[130].

1.6 Rationale

Through linkage analysis and homozygosity by descent analysis, followed by NGS (next generation sequencing), and computational analysis, variants in *HYAL2* causing K148R and P250L substitutions were identified as a putative cause of cleft palate in subjects of Amish and Saudi Arabian descent[44]. The reduced genetic heterogeneity in these populations facilitates the identification of disease genes but also increases the probability of identifying homozygous changes that are not the cause of disease, but are instead in linkage disequilibrium with the disease because they are closely located to the causative mutation. Therefore, assessing the

impact of these variants on the function of HYAL2 is important to confirm these mutations as causative. A second approach to determine if these mutations were the likely cause of the disease was by comparing the phenotypes of the human patients with that of the *Hyal2* KO mice. Affected individuals exhibited craniofacial abnormalities, including cleft palate and/or lip, cardiac abnormalities, myopia and hearing loss. A comparison of the HYAL2-deficient patients with the *Hyal2* KO mice demonstrated many similarities in the phenotypes, including craniofacial dysmorphism, cleft palate (submucosal with underdeveloped viscerocranial bones in mice), heart abnormalities, and hearing loss[44].

The exact role of HYAL2 in HA regulation during cellular differentiation is yet to be determined. HYAL2-deficient mesenchymal cells in the palate are expected to have increased proliferation but decreased differentiation due to elevated HA levels and/or size. In previous studies, we have detected an overabundance of HA in different tissues of the *Hyal2* KO mouse[42]. In cardiac cushion explant experiments it was shown that high molecular mass HA promoted EMT while small fragments of HA inhibited EMT signaling and promoted differentiation[131]. A similar phenomenon has been reported during palatogenesis which shows that, after the palatal shelf elevation, there is a decline in HA content[132], suggesting that as in the heart, HYALs may be required to remove HA to inhibit proliferation of mesenchymal cells and promote differentiation[131]. HA provides turgor pressure for palatal shelf elevation[97] and produces large intercellular spaces to prevent cell-cell and cell-matrix interactions to allow assembly of extracellular constituents. Low molecular mass HA has been shown to promote osteogenesis *in vitro*.[133] An analysis of the morphology of the developing palate and a qualitative evaluation of the proliferation and differentiation of mesenchymal cells within the palate region would provide

an important basis for further studies aimed at determining the role of HYAL2 in palate development.

1.7 Research Aims

1. To determine if the K148R and P250L mutations cause HYAL2 deficiency.

2. To examine the morphology of the developing palate in HYAL2 KO mice.

3. To qualitatively assess bone development of the HYAL2 KO palate.

1.8 Hypothesis

We hypothesize that HYAL2 mutations associated with cleft palate result in HYAL2 deficiency, and increased HA in the craniofacial region is associated with decreased bone formation in HYAL2 KO palate.

Chapter 2: Materials and Methods

2.1 Generation of a homology model of HYAL2

The amino acid sequence of human HYAL2 (NCBI Ref: NP_149348.2) was used in a BLAST[134] search for homologues in the PDB (protein databank) sequence database. The crystal structure of HYAL1 (PDB ID: 2PE4)[25] was identified as a suitable template for homology modeling of HYAL2 using the I-TASSER server.[135] For building the enzyme/substrate complex of HYAL2, the existing crystal structure of bee venom hyaluronidase complexed with a tetramer of HA (PDB ID: 1FCV)[136] was used as an overlay on the HYAL2 model. The sugar units of the tetrameric HA from the bee venom structure were placed into the sugar binding sites of the active site groove at positions designated -1 through -4. The substrate distortion which is reported to take place in the -1 subsite of the retaining glycosidases[137] was introduced by placing the non-reducing GlcNAc of a correctly distorted chitobiose disaccharide (from a crystal structure of a chitobiase from *Serratia marcescens* [PDB ID: 1QBB])[138] into the -1 subsite of HYAL2 which replaced the previously superimposed terminal GlcNAc of the HA tetramer into the -1 subsite. For making the HA hexamer bound to HYAL2, the reducing GlcNAc of the chitobiose molecule (now bound in the +1 subsite of HYAL2) was converted into a GlcUA sugar and terminal GlcNAc was then added to the GlcUA in the +1 subsite via a β(1->3) linage and fit into the putative +2 subsite of HYAL2. All the superimposition and conversion of the sugar molecules was done using The PyMOL Molecular Graphics System, Version 1.3 Schrödinger, LLC[139].

2.2 Modeling of the mutations

The prediction of the location and possible effects of mutations for the amino acid substitutions was modeled using the mutagenesis program in PyMoL Molecular Graphics System. First, the PDB file of the predicted HYAL2 structure was uploaded into PyMoL, and the position of the amino acid was visualized using the mutagenesis program. The amino acids lysine (K) 148 and proline (P) 250 were changed to arginine (R) and leucine (L) respectively. The replacement of the amino acids in the PDB structure of HYAL2 introduced rotamers (several side chain orientations) that affect the favorable position of the amino acid and might impact the interaction of these residues with other amino acids. The most favorable rotamers for the amino acid substitutions were manually selected and the mutated HYAL2 was superimposed over the wild type using the alignment tool.

2.3 Construction of human HYAL2 and HYAL1 expression vectors

A commercial mammalian expression vector pCMV6-XL5 containing the full-length HYAL2 cDNA (NM_003773) was purchased from Origene (Cat # SC117754). The c.443A>G p.K148R and c.749C>T p.P250L HYAL2 mutations identified in Amish and Saudi Arabian subjects, respectively, were introduced into the *HYAL2* sequence by fusion PCR. In short, the complementary primers specifying the single nucleotide mutation were used in combination with outer primers from the *Hyal2* sequence to generate two different PCR products containing the mutation using Phusion polymerase (New England BioLabs). The two PCR products were then separated by agarose gel electrophoresis and purified using a GeneJET agarose gel extraction kit (ThermoFisher). The isolated fragments were then used as templates for PCR amplification with the same outer primers using high-fidelity DNA polymerase Phusion polymerase (Thermo

Scientific) or KAPA HiFi DNA Polymerase (Kappa Biosystems). Similar fusion PCR strategy was applied to introduce the HYAL1 c.431A>G p.K144R (NM_153281) mutation equivalent of the K148R mutation in HYAL2. First, a full-length HYAL1 expression vector was prepared by PCR-amplification of EST clone 937230 (GenBank AA223264.1) using *HYAL1* outer primers for 32 cycles of 30 seconds at 94ºC, and 1 min each at 59ºC and 72ºC. The resulting 1.3 kb PCR product was restriction enzyme digested with BamHI and EcoRI, and ligated into BamHI/EcoRI digested pIRESneo vector (BD Biosciences) to generate pIRES_HYAL1. Thus, point mutations were introduced into the *HYAL2* and *HYAL1* sequences for the functional assay.

Table 2. 1 Primers used to introduce HYAL2 and HYAL1 mutations.

The bases that were changed to introduce the single base substitutions are shown in capital letters.

Targeted Mutation	Primer sequence
HYAL2 c.443A>G p.K148R	5'-actggcaggacaGagatgtgtatcg-3'(forward)
	5'-cgatacacatctCtgtcctgccagt-3'(reverse)
HYAL2 c.749C>T p.P250L	5'-acggccctcttccTgtctgtc-3'(forward)
	5'- gacagacAggaagagggccgt-3'(reverse)
HYAL1 K144R	5'-tgggacaccaGggacatttaccg-3'(forward)
	5'-cggtaaatgtccCtggtgtccca-3' (reverse)
HYAL2 Outer Primers	5'-atgcgggcaggcccaggcccacc-3'(forward)
	5'- gctacaaggtccaggtaaaggcca-3'(reverse)
HYAL1 Outer Primers	5'-gcggaattctgccatggcagcccacctgctt-3' (forward)
	5'- gcggatccaatcaccacatgctcttccgc-3' (reverse)

2.4 Restriction enzyme digestion

The fusion PCR product originating from the second PCR (above) was then inserted into the vector by restriction enzyme digestion followed by ligation. Restriction enzyme Fast Digest EcoRI (ThermoFisher) and ApaI (New England Biolabs) were used to digest the plasmid DNA or the PCR product following the standard digestion protocol. For restriction enzyme digestion, 0.1-0.5 µg of plasmid DNA or 0.1-0.3 µg of PCR product, 1 µl of 10X restriction enzyme buffer and 1-2 U of restriction enzyme was used in a total volume of 10 µl. A one-h incubation for the restriction enzyme digestion was done for EcoRI and ApaI (for HYAL2) and BamHI and EcoRI

(for HYAL1) at 37ºC and 25ºC respectively. Restriction digestion was stopped by heat inactivation of the enzymes at 65ºC for 20 min. Following restriction digestion, dephosphorylation of the plasmid DNA was done to inhibit the re-circularization of the linearized plasmid. For the dephosphorylation reaction, 2 µl of 10X Antarctic Phosphatase Reaction Buffer and 5 U Antarctic Phosphatase (New England BioLabs) was added to the digest, and the total volume was increased to 20 µl. This reaction was incubated at 37ºC for 30 min and stopped by heat-inactivation at 80ºC for 2 min.

2.5 Ligation

pCMV6-XL5 and pIRESneo vector (BD Biosciences) vectors were digested with EcoRI/ApaI (for HYAL2) and BamHI/EcoRI (for HYAL1). Restriction digestion created sticky ends in the plasmid and insert DNA. Ligation of the mutated *HYAL2* and *HYAL1* DNA fragment with the plasmid was done at different vector: insert ratios. Each ligation reaction contained 2 µl of 10X T_4 DNA ligase buffer, different concentrations of the plasmid and insert DNA (~30-50 ng plasmid DNA, ~30-40 ng insert DNA), and 1 µl of the T_4 DNA ligase in a total volume of 20 µl. The ligation reaction was incubated for 1 h at room temperature and stopped by heat-inactivation at 65ºC for 10 min.

2.6 Transformation of *Escherichia coli*

For transformation, electrocompetent *Escherichia coli* (DH5α) were used. One µl of the ligation mixture was added to 40 µl of *E. coli* in a chilled 0.1 mm electroporation cuvette. Using a BTX Cell Manipulator, electroporation was performed using the following settings 1.3KV, 129 Ω, 50 µF and immediately mixed with 960 µl of prewarmed SOC (0.5% yeast extract, 2% tryptone, 10

mM NaCl, 2.5 mM KCl, 10 mM $MgCl_2$, 10 mM $MgSO_4$, 20 mM glucose) broth. This was followed by 1 h incubation at 37°C. Aliquots (50 and 100 µl) of the transformation mixture were plated onto Miller's LB agar containing 100 µg/ml ampicillin and incubated overnight at 37°C. The following day, individual colonies from the agar plate were sub-cultured into 3 ml LB broth containing 100 µg/ml ampicillin (LBA) and incubated with shaking at 37°C overnight. These cultures were used for plasmid isolation.

2.7 Plasmid isolation

Plasmids were isolated using a NucleoSpin® Plasmid kit (Macherey-Nagel) as per the manufacturer's instruction. In summary, 2 ml of *E. coli* LBA overnight culture was pelleted by a short centrifugation, and the supernatant was removed. Bacterial cell pellets were then resuspended in the buffer provided in the kit followed by liberating the plasmids by lysing the cells with sodium dodecyl sulfate (SDS)/alkaline lysis buffer. Following this, the alkaline solution of the extracted plasmid was neutralized with another buffer and prepared for binding with the silica membrane provided with the plasmid isolation column kit. By centrifugation, precipitated proteins, genomic DNA, and cell debris were removed before running through another column and washed with an ethanolic buffer. Finally, the silica membrane was dried, and the plasmid DNA was eluted with slightly alkaline buffer.

2.8 Sequencing

To confirm error-free construction of the mutated *Hyal2* constructs during PCR amplification, the *Hyal2* coding regions from the constructs were fully sequenced at the Toronto Centre for

Applied Genomics. The concentrations of the *HYAL2* wild-type and mutated plasmids were approximately 400 ng/µl, and the β-Gal plasmid had a concentration of about 1.7 µg/µl.

2.9 Culture of mouse embryonic fibroblasts

Mouse embryonic fibroblasts (MEFs) deficient in HYAL2 or HYAL1 were derived from *Hyal2*^{-/-} or *Hyal1*^{-/-} embryos as part of previous studies[12,42]. These cells were transfected with a vector expressing the large T antigen to immortalize the cells. MEFs were grown in 6 well culture dishes with Dulbecco's Modified Eagle's Medium (DMEM) containing 10% serum. Cells were incubated in 5% CO_2 at 37°C until they reached ~90-95% confluency.

2.10 Transfection of MEFs

DNA for transfection was prepared by equalizing the concentration of wild-type, K148R, and P250L plasmids. The concentration of the plasmid was measured by both *NanoDrop™* and by comparison of the intensities of the bands to a DNA mass ladder after separation on an agarose gel. MEFs were grown to 90% confluency on the day of transfection. Cells were washed with PBS (1.1 mM KH_2PO_4, 8.1 mM Na_2HPO_4, 2.7 mM KCl, 138 mM NaCl, pH 7.6) and transfection was done using TurboFect Transfection Reagent (Thermo Scientific) and following the protocol recommended by the manufacturer. For the analysis of the transgene expression, the cells and media were collected 48 h post transfection. Cells were washed three times with phosphate buffered saline (PBS), and then the cells were scraped from the culture plate into 250 µl of PBS containing a 1:500 dilution of a protease inhibitor cocktail (Sigma). Cell lysates were prepared by sonication using a Sonic Dismembrator 100 (Fisher Scientific) at 15 amplitudes and giving 2 bursts of 5 S each on ice with a 30 S interval between bursts.

2.11 Protein quantification

The protein concentration of the transfected cell lysates was determined using the Bradford assay. In this assay, 1µg/µl of bovine gamma globulin was used to prepare a standard curve for the interpretation of the protein concentration in the experimental samples. For each sample, 2 µl of the cell extract was added to 200 µl of Bradford reagent (BioRad) followed by adding 798 µl of water. This mixture was incubated at room temperature for five min, and the absorbance was read using an Ultrospec 1000 spectrophotometer at 595 nm. As a control, 2 µl of lysis buffer was added to 798 µl of water and mixed with 200 µl of Bradford reagent to assay the background produced from the cell lysates. Each of the experimental samples was analyzed in duplicate and compared to the absorbance of samples of known protein concentration.

2.12 β-galactosidase activity assay

β-Galactosidase activity was determined by incubating the substrate o-nitrophenyl-β-D-galactopyranoside (ONPG) with an aliquot of the cell lysate containing 25 µg of protein. This mixture produced a yellow colored product, o-nitrophenyl, from the enzymatic activity of the β-galactosidase enzyme. In summary, a volume equivalent to 25 µg of protein from each cell lysate was added to 25 µl of PBS followed by water to make the final volume up to 150 µl. The diluted cell lysate was then mixed with 150 µl of Z buffer (120 mM Na_2HPO_4, 50 mM NaH_2PO_4, 2 mM $MgCl_2$, 100 mM β-mercaptoethanol, 1.33 mg/ml ONPG). The reaction mix was then incubated for 30 min at 37°C to allow the formation of the yellow color in the presence of β-galactosidase. The reaction was stopped by adding 500 µl of 1 M sodium carbonate, and the absorbance was read at 420 nm using a spectrophotometer. The specific β-galactosidase activity (absorbance unit/30min/µg of protein) was used to estimate the transfection efficiency. This β-galactosidase

activity was used to normalize the co-expressed HYAL2 expression level. The normalization was done by calculating a correction by making the average β-galactosidase specific activity of the samples in a transfection equal one and converting the β-galactosidase specific activity of each sample to a portion of one.

2.13 Western blot analysis of the expressed proteins

For western blot analysis of the expression level of mutant and wild-type HYAL2, aliquots of the transfection lysates, normalized based on β-galactosidase activity, were separated by SDS-polyacrylamide gel electrophoresis (PAGE) as follows. Polyacrylamide gels were cast using 7.5% acrylamide as the resolving gel (40 mM Tris pH 8.8, 0.1% SDS, 7.5% to 10% polyacrylamide [29:1 acrylamide: bisacrylamide], 0.1% tetramethylethylenediamine (TEMED), 0.075% ammonium persulfate). Following polymerization of the resolving gel, a 4% stacking gel (60 mM Tris pH 6.8, 0.1% SDS, 4% polyacrylamide, 0.1% ammonium persulfate, 0.01% TEMED) was poured, and a comb was inserted. Next, based on the β-galactosidase assay to correct the protein concentration, normalized volumes (15-20 µl) of cell lysates (20-25 µg of protein) were mixed with sample prep buffer (8% SDS, 250 mM Tris pH 6.8, 40% glycerol, 0.01% bromophenol blue, 400 mM dithiothreitol), and boiled for 5 min followed by cooling and a short centrifugation. The tank was filled with running buffer (25 mM Tris, 192 mM glycine, 0.1% SDS) and the gel was run at 160 V for approximately 1 h, or until the bromophenol blue marker in the loading buffer reached the bottom of the gel. Following separation of proteins by SDS-PAGE, the gel was equilibrated in ice-cold Tris-glycine transfer buffer (80% running buffer, 20% methanol) for 15 min. The proteins were then transferred to a nitrocellulose

membrane (Bio-Rad) at 100 V for 1 h at 4°C. After transfer, total protein was visualized by rinsing the membrane with Ponceau S (0.1% Ponceau S in 5% acetic acid).

For the antibody detection of the protein on the nitrocellulose membrane, it was blocked in 5% skim milk in Tris-buffered saline Tween (TBST) (20 mM Tris pH 7.4; 0.15 M NaCl; 0.1% Tween 20) for one h. HYAL2 was detected using anti-HYAL2 primary antibody (Proteintech, Cat #15115-1-AP) diluted (1:500) in 5% skim milk powder in TBST overnight at 4°C. For detection of HYAL1, a monoclonal anti-HYAL1 antibody, 1D10 was used as previously described[12]. The following day, blots were washed three times with TBST, incubated with horseradish peroxidase (HRP)-conjugated secondary donkey anti-rabbit antibody for one h, washed, and visualized using Immobilon western chemiluminescent HRP substrate (Millipore). The light signal from the blot was detected for 5 S to 10 min using a ChemiDoc™ MP Imaging System (BioRad). The chemiluminescent signal from the expressed proteins was quantified using Image Lab™ software. For quantification of the signal, the lane frame was resized manually for each lane area, and the band was detected using the automatic band detection tool. Next, the quantification tool was used to determine the light emitted (light units) from each band. These were manually normalized to the wild-type levels of HYAL2 for each blot.

2.14 HA binding assay

The binding of HA to HYAL2 was measured using the ability of the cationic detergent hexadecylpyridinium chloride (CPC) to bind with negatively charged molecules such as HA and other associated molecules to make an insoluble complex. For this procedure, 20-30 µg of HYAL2 transfected cell lysate (normalized based on β-galactosidase activity) was mixed with 50 µl of RIPA buffer (1% Igepal, 0.5% Na-deoxycholate, 0.1% SDS in PBS), incubated on ice for

30 min, and then sonicated as described earlier. Cell lysates were then collected and centrifuged at 17,000 rpm for 10 min. Supernatants were collected, and the protein concentration was determined using the Bradford assay as previously described. Next, 50 µg of (50 µl of 1 mg/ml) commercial HA was added to the reaction and incubated overnight with rotation at 4ºC. The following day, 100 µl of 2% CPC was added to the reaction mix and incubated at 37ºC for 90 min followed by centrifugation at 17,000 rpm for 10 min. The supernatant was then discarded from the tube, and 500 µl of 1% CPC wash buffer (30 mM NaCl, 1% CPC in water) was added, centrifuged for 2 min at 17,000 rpm, and the supernatant was discarded. Finally, the pellets were thoroughly mixed with 300 µl of SDS-PAGE sample loading buffer and analyzed for HYAL2 by western blot analysis using the anti-HYAL2 antibody as described above.

2.15 Zymography and enzyme activity measurement

Zymography was done with a minor modification of the earlier method described by Guntenhoner et al.[16] In summary, a 1:10 dilution of the transfected cell lysate and media was prepared in tris-buffered saline with 1% Triton X-100. Diluted samples were then loaded on a 7% polyacrylamide gel (containing 0.18 mg/ml of rooster comb HA) and separated under native conditions. Following electrophoresis, the gel was incubated overnight at 37°C in 0.1 M formate buffer containing 0.15 M NaCl at pH 3.8. After the first incubation, the gel was washed briefly with distilled water and continued for a second incubation with 20 mM Tris pH 8.0 containing 0.02 mg/ml of Proteinase K (Sigma) for 4 h at 37°C. Later, the gel was rinsed with distilled water and incubated in 7% acetic acid for 15 min. HA staining of the gel was done by incubating with 3% acetic acid, pH 2.5 containing 1% Alcian blue 8GX for 30 min. Finally, the gel was destained in 7% acetic acid and then counterstained in Coomassie Blue G250 for 10 min

followed by destaining (30% methanol, 7% acetic acid) until clearing of the gel was apparent. A modified Reissig assay was done for the quantification of the hyaluronidase activity from the media[140]. After 48h of transfection, media was collected and incubated for 18h at 37^0C with buffer containing 0.1M Na formate, 0.1M NaCl, 100 µg HA, 1.5 mM saccharic acid lactone. The reaction was terminated by adding borate buffer (0.8M K^+-tetraborate), and samples were boiled for 3 min and allowed to cool at room temperature. DMAB (p-dimethylaminobenzaldehyde) was added for a final incubation for 20 min at 37^0C. Finally, samples were briefly centrifuged and read at 585 nm using a spectrophotometer.

2.16 *Hyal2+/+* and *Hyal2-/-* knockout mouse sample collection and genotyping

As part of an earlier study[41], mice deficient in HYAL2 were maintained on a mixed 129/Ola/CD1/C57BL/6 background. In this study, all procedures regarding the care of the animals were done complying with the Canadian Council on Animal Care and approved by the Animal Protocol Management and Review Committee at the University of Manitoba. When the timed pregnant mice reached their pre-determined endpoint for embryo collection, they were euthanized by isoflurane overdose and immediately dissected. Each embryo was then collected separately from the uterus and washed with PBS. Heads from the embryos were fixed in 10% formalin (Fisher Scientific) containing 0.5% CPC (Sigma) overnight at room temperature, and tissue from the body was collected for genotyping. The tissues were then washed three times for 5 min in PBS and once in 70% ethanol for 5 min prior to being stored in 70% ethanol until processing. Decalcification of the embryos from E15.5-17.5 was completed by incubation in Immunocal (Decal Chemical Corporation) overnight. Tissues were then stored in 70% ethanol

until processing. PCR based genotyping was done from the DNA samples isolated from embryos collected from E14.5-E19.5 as described earlier.[42]

2.17 Tissue processing, embedding, and microtomy

The tissues fixed in the 10% buffered formalin were processed in a Citadel 1000 tissue processor under vacuum. Tissue dehydration was done in 70% ethanol for 1 h, 95% ethanol for 3 h, 100% ethanol for 6 h, and xylene for 2.5 h. Following dehydration, the tissues were equilibrated in two melted paraffin solutions for 6 h. After completion of the tissue processing, embedding to make paraffin blocks was done in a Histocentre 3 embedder. Finally, 5 μm tissue sections were cut using a Leica RM2245 microtome, and sections were adhered to glass slides.

2.18 Histological staining

2.18.1 Hematoxylin and eosin (H&E) staining

Tissue sections were deparaffinized by incubating in two changes of xylene for 5 min, 100% ethanol for 5 min and 95% ethanol for three min. This was followed by washing in 70% ethanol for three min, 50% ethanol for three min and finally in water for three min. Slides were then stained for 3 min in Mayer's hematoxylin (Sigma) followed by washing under running tap water for 6 min. Slides were then rehydrated using decreasing concentrations of ethanol. Next, the slides were transferred to 80% ethanol for 1 min and then incubated for 40 sec in Eosin Y stain (Sigma). This was followed by 3 min incubation in 70% ethanol followed by increasing concentrations of ethanol, and finally by xylene. The slides were then mounted in a toluene-based mounting medium, Permount (Fisher Scientific) and visualized using light microscopy. Images were taken using AxioVision software.

2.18.2 Detection of HA

HA in the palate was detected using a biotinylated HA-binding protein (HABP; Calbiochem) as described but without enzyme retrieval[27]. To assess the HABP specificity, control slides were prepared in parallel to the experimental slides. The control slides were incubated overnight at 37^0C with 50 U/ml hyaluronidase from *Streptomyces hyalurolyticus* (Sigma) in sodium acetate pH 6.0 before the HABP detection. Following overnight incubation, tissue sections were washed with PBS and incubated with 3% hydrogen peroxide in distilled water for 30 min for quenching endogenous peroxidases. Next, tissue sections were washed by PBS and incubated for 30 min in 10% Fetal Bovine Serum in Tris Buffered Saline Tween (TBST; 50 mM Tris, 150 mM NaCl, 0.1% Tween 20, pH 7.4). According to the instructions of the manufacturer (Vector Laboratories) incubation with avidin D followed by biotin was done to block endogenous biotin. In the next step, the slides were washed in TBST and incubated overnight at 4°C with a biotinylated-HABP (Calbiochem) at a concentration of 6.67 µg/ml in TBST. Next day, the slides were washed in TBST and incubated with avidin-horseradish peroxidase complex (Vector Laboratories) for 1 h and detected with diaminobenzidine (DAB). The DAB substrate (prepared without nickel) was made before application according to the manufacturer's protocol (Vector Laboratories). Later, the slides were washed in water and counter stained with 0.1% Nuclear Fast Red.

2.18.3 Alkaline phosphatase staining

Formalin-fixed tissue samples (described above) were decalcified using Immunocal (Decal Chemical Corporation) by overnight incubation followed by washing as per the manufacturer's instruction. Decalcified tissues were then processed, embedded and sectioned as described in

section 2.17. Alkaline phosphatase activity in both the *Hyal2+/+* and *Hyal2-/-* palate sections was detected with minor modification of a previously described procedure[141]. In short, slides were deparaffinized and treated with a series of xylene and decreasing grade of alcohol incubations followed by overnight incubation at 4°C in 1% magnesium chloride in 100 mM Tris-maleate buffer pH 9.2. Next, the sections were incubated for 2 h with a freshly prepared alkaline phosphatase substrate solution containing 100 mM Tris-maleate buffer, pH 9.2, containing 0.2 mg/ml naphthol AS-MX phosphate and 0.4 mg/ml Fast Red TR. After incubation sections were washed in distilled water and counterstained with Vector methyl green nuclear (Vector Laboratories) followed by mounting with a toluene based solution. Finally, microscopy and imaging were done for further analysis.

2.18.4 Immunohistochemistry

Formaldehyde-fixed, paraffin-embedded tissues mounted on slides were deparaffinized and rehydrated as for H & E staining. For antigen retrieval, deparaffinized slides were incubated in preheated 10 mM sodium citrate buffer (pH 6.0) at ~95°C by placing in a boiling water bath for 20 min. The slides were then cooled in the citrate buffer for 20 min at room temperature. In the next step, the endogenous peroxidases were quenched by washing the slides twice in distilled water for five min each and treated with 3% H_2O_2 for 10 min. Following H_2O_2 treatment, the slides were washed in TBST for five min, a circle was made around the section using a hydrophobic slide marker (Research Products International) and sections were blocked in 3% BSA in TBST for 60 min at room temperature. An avidin-biotin blocking kit (Vector Labs) was used to block endogenous biotin using the following the manufacturer's instructions. Next, slides were washed in TBST for two min, and the sections were incubated with a primary antibody in

blocking solution overnight at 4°C in a humidified chamber. See table 2.2 for the list of antibodies used. The next day, slides were rinsed three times in TBST for five min each, and incubated with biotinylated secondary antibody for 1 h at room temperature. While incubating with secondary antibody, the ABC complex (Vector Labs) containing horseradish peroxidase was prepared by adding 1 drop of solution A and 1 drop of solution B into 5 ml TBST. The slides were washed three times for two min in TBST, and incubated in a drop of the prepared ABC complex for 1 h, followed by washing the slides three times for two min in TBST. After washing, each section was treated with one drop of diaminobenzidine (DAB) substrate (Vector Labs), and incubated for ten min at room temperature to allow a brown precipitate to form. This was followed by washing twice in water for five min each. The washed slides were next counterstained with Nuclear Fast Red (ScyTek Lab.) to stain the nuclei. Finally, the slides were dehydrated by incubating with 50% ethanol for 3 min, 70% ethanol for three min, two times 95% ethanol for three min each, two times in 100% ethanol for five min and finally twice with xylene for five min each. Slides were then mounted with Permount, visualized, and imaged as described above.

Table 2. 2 List of antibodies

Primary antibodies			
Identity	**Source**	**Catalog No.**	**Application**
Anti-Osterix/	Rabbit polyclonal	AB22552 (Abcam)	1 in 800
Anti-Periostin	Rabbit polyclonal	AB614041 (Abcam)	1 in 500
Secondary antibodies			
Goat anti-rabbit biotinylated	Goat	BA-1000 (Vector Lab.)	1 in 500

2.19 EMT microarray analysis

For EMT gene expression analysis tissues from the nasopharynx of E12.5 *Hyal2+/+* and *Hyal2-/-* embryos were collected. RNA from the sample was isolated using RNeasy plus Mini Kit (QIAGEN) following manufacturer's instruction. RNA concentration was measured using *NanoDrop™*. Maxima First Strand cDNA Synthesis Kit for RT-qPCR (Thermo Fisher) was used for cDNA synthesis using the following reaction mixture: 50 ng of the template RNA, 4µl 5X Reaction mix, 2 µl Maxima Enzyme Mix making up to 20 µl of total volume with nuclease-free water. In this experiment, two different negative control was used where no enzyme and template was provided into the reaction mix. All the experimental and negative control samples were incubated for 10 min at 25^0C followed by 60 min incubation at 50^0C. The cDNA synthesis

reaction was stopped by heating the samples at 85^0C for 5 min. PrimeTime® assay was purchased from IDT in 2-96 well plates. Each assay was prepared as 4 identical replicates of 2 µl probes and primers for the gene expression study of 45 genes (42 genes for EMT and HA metabolism with 3 endogenous control genes as shown in Table 2.3). EMT related genes and their targets used in this experiment are enlisted in the appendix I. 10 µl of the PrimeTime® gene expression master mix from IDT containing the reference dye was mixed with 8 µl of the template (1/50 dilution of the cDNA) for the 20 µl reaction Prime Time assay. Applied Biosystems® 7500 Real-Time PCR Systems was used for analyzing the gene expression from this assay. Expression of genes was analyzed in duplicate, normalized to three endogenous controls, and averaged. The ΔΔCT was then determined by comparing the knockout to the wild-type samples and converting the result to fold change relative to the wild-type sample.

Table 2. 3 Genes analyzed in PrimeTime® expression arrays.
Genes related to HA metabolism and endogenous controls are highlighted as blue and green respectively.

Nodal	*Tgfb1*	*Hyal2*	*Notch1*	*Egfr*	*Cd44*	*Smad2*	*Pdgfrb*
Stab2	*Tgfb2*	*Zeb1*	*Lyve1*	*Tgfb3*	*Ctnb1*	*Hyal1*	*Wnt11*
Stat3	*Hmmr*	*Rac1*	*Vegfa*	*Has2*	*B2m*	*Gusb*	*ActB*
Cdh2	*Sox10*	*Ocln*	*Col1a2*	*Twist1*	*Fgfbp1*	*Fn1*	*Vdcan*
Akt1	*Mmp2*	*Cdh1*	*Bmp1*	*Mmp9*	*Vim*	*Mmp7*	*Snai1*
Wnt5a	*Erbb3*	*Snai2*	*Wnt5b*	*Msn*	*B2m*	*Gusb*	*ActB*

2.19 Statistics

Comparisons between experimental groups were performed using unpaired T-test and ANOVA test by using GraphPad Prism software. Error bars shown in graphs represent the standard error of the mean.

Chapter 3: Results I

Expression of Putative HYAL2 Disease-Causing Mutations

3.1 Introduction

A *HYAL2* mutation NM_003773.4: c.443A>G;p.K148R was identified as the putative cause of syndromic cleft lip and palate in Amish patients using an identity by descent strategy followed by exome sequencing[44]. However, further confirmation of the causative nature of this mutation required analysis of its impact on the HYAL2 protein. During the course of these studies, a second *HYAL2* mutation, NM_003773.4: c.749C>T;p.P250L identified in Saudi Arabian patients, was also incorporated into our analysis of the impact on HYAL2. In both cases, although the genetic evidence was strong, there was still a possibility that additional mutations in close proximity to *HYAL2*, which were not identified by exome sequencing, could be the cause of the syndrome. We used a combination of homology comparisons and modeling, as well as protein expression, to analyze the impact of the K148R and P250L mutations on HYAL2.

3.2 Conservation of the K148R and P250L residues

The amino acid sequence predicted from the *HYAL2* cDNA sequence NM_003773.4 was used in a BLAST[134] search for related sequences in NCBI GenBank that could be used in a multiple sequence alignment. The coding sequence of the four known human homologues (*HYAL1*, *HYAL3*, *HYAL4*, and *PH-20* (*SPAM1*)), as well as that of murine and bovine *HYAL2*, and the more distantly related bee venom, *C. elegans*, scorpion and snake hyaluronidases were selected for the multiple alignment (Table 3.1).

Table 3. 1 List of proteins used for alignment in Fig. 3.1

Protein name	GenBank Sequence number
Human HYAL2	NP_003764.3
Mouse HYAL2	NP_034619.2
Human HYAL1	NP_149349.2
Human HYAL3	NP_003540.2
Human HYAL4	NP_036401.2
Sperm hyaluronidase	NP_694859.1
Bee venom-HYAL2	NP_001011619.1
C.elegans-HYAL2	NP_495830.1
Scorpion-HYAL2	XP_015922490.1
Snake-HYAL2	XP_015677767.1
Bovine-HYAL2	NP_776772.1

An alignment was done among the hyaluronidase homologs in Table 3.1 using CLUSTAL X[142] to assess the sequence conservation at the amino acid at positions 148 and 250 (Fig.3.1). The PDB sequence of HYAL1, 2PE4, was also used in the alignment to compare the predicted secondary structure characteristics (Fig. 3.1).
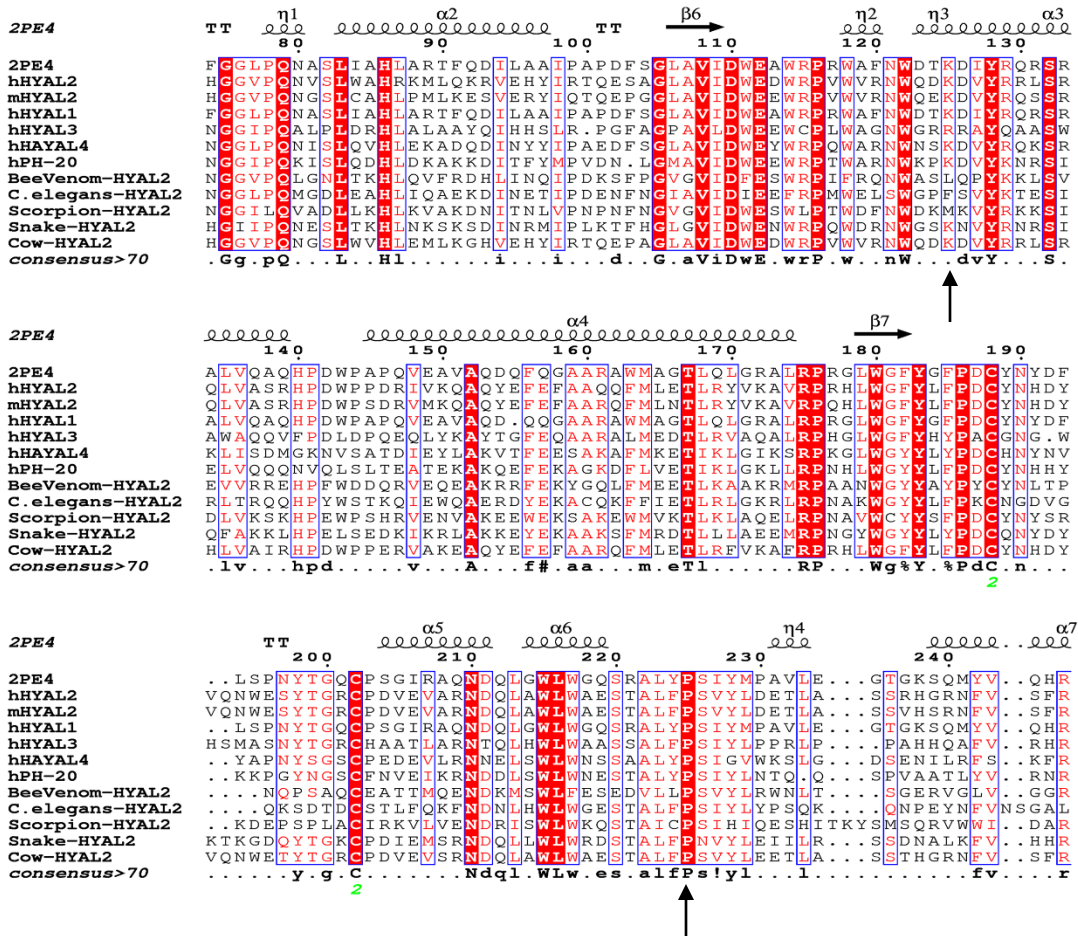
Figure 3. 1 Multiple sequence alignment of hyaluronidases.

Alignment of the HYAL1 amino acid sequence (PDB 2PE4) with other hyaluronidase-related proteins as well as the HYAL2 amino acid sequence from several species. Numbering is based on the HYAL1 (2PE4) sequence. The secondary structure of the proteins is predicted based on the alignment to the template 2PE4. The position of the K148 and P250 residues are indicated with black arrows. Amino acid sequence consensus of more than 70% is shown for the alignment where uppercase indicates identity, and lowercase represents a consensus level of >50%[143].

The alignment showed that the K at position 148 was conserved in most of the mammalian hyaluronidases, although an R substitutes it in HYAL3, an enzyme for which no function has currently been assigned.[144] The P at position 250 was completely conserved in all of the aligned sequences and fell in a highly-conserved region of the protein (Fig. 3.1). Both residues were conserved in its more active paralogue, HYAL1. Therefore, it was apparent that both residues were conserved, but further analysis was required in order to try to determine the impact of these substitutions on HYAL2 structure.

3.3 Comparative modeling of HYAL2

The availability of the crystal structure of HYAL1 (2PE4), which would serve as a template, made homology modeling of HYAL2 possible. As a first step, guided by the multiple alignment of a subset of the sequences in Fig. 3.1, a two-way alignment of HYAL1 and HYAL2 protein sequences was generated (Fig. 3.2) to use in the preparation of a homology-based model (Fig. 3.3). The alignment was then used to generate a comparative molecular model based on the crystal structure of HYAL1 using the I-Tasser program.[135] The homology model of hHYAL2 predicted the expected enzyme-substrate complex that could form between HYAL2 and HA before the cleavage of the glycosidic bond in HA. An overall surface representation of the HYAL2 model is shown in grey (Fig. 3.3A). The HA hexamer bound within the active site groove is shown in stick format using green carbons, the position of the Lys148 and Pro250 residues are shown in stick format and labeled in green and purple respectively (Fig. 3.3 B). The cartoon representation of HYAL2 (Fig. 3.3 C and D) shows the position of the both Lys148Arg and Pro250Leu wild type and mutated residues (wild type, grey; mutated orange).

The K148 and P250 residues are labeled in orange. In the predicted model the K148 residue is located within ~4Å of the HA substrate which suggests this K could interact with the HA bound in the active site of HYAL2. The mutation from K148 to R results in a longer side chain compared to Lys that might be expected to distort the shape of the subsite in this position, resulting in reduced substrate binding affinity and less catalytic activity. The P250 residue was deeply buried below the active site in the predicted structure of HYAL2. The position and electrostatic binding partners of the P250 molecule suggested that mutations in this position might distort the structural integrity of the overall protein. Thus, the P250L mutation might impact the folding and stability of HYAL2.

```
HYAL2              MRAGPGPTVTLALVLA-VSWAMELKPTAPPIFTGRPFV  37
HYAL1                 MAAHLLPICALFLTLLDMAQGFRGPLLPNRPFT  33


HYAL2   VAWDVPTQDCGPRLKVPLDLNAFDVQASPNEGFVNQNITIFYRDRLGLYP  87
HYAL1   TVWNANTQWCLERHGVDVDVSVFDVVANPGQTFRGPDMTIFYSSQLGTYP  83


HYAL2   RFDSAGRSVHGGVPQNVSLWAHRKMLQKRVEHYIRTQESAGLAVIDWEDW  137
HYAL1   YYTPTGEPVFGGLPQNASLIAHLARTFQDILAAIPAPDFSGLAVIDWEAW  133


HYAl2   RPVWVRNWQDKDVYRRLSRQLVASRHPDWPPDRIVKQAQYEFEFAAQQFM  187
HYAL1   RPRWAFNWDTKDIYRQRSRALVQAQHPDWPAPQVEAVAQDQFQGAARAWM  183


HYAL2   LETLRYVKAVRPRHLWGFYLFPDCYNHDYVQNWESYTGRCPDVEVARNDQ  237
HYAL1   AGTLQLGRALRPRGLWGFYGFPDCYN--YDFLSPNYTGQCPSGIRAQNDQ  231


HYAL2   LAWLWAESTALFPSVYLDETLASSRHGRNFVSFRVQEALRVARTHHANHA  287
HYAL1   LGWLWGQSRALYPSIYMPAVLEGTGKSQMYVQHRVAEAFRVAVAAGDPN-  280


HYAL2   LPVYVFTRPTYSRRLTGLSEMDLISTIGESAALGAAGVILWGDAGYTTST  337
HYAL1   LPVLPYVQIFYDTTNHFLPLDELEHSLGESAAQGAAGVVLWVSWENTRTK  330


HYAL2   ETCQYLKDYLTRLLVPYVVNVSWATQYCSRAQCHGHGRCVRRNPSASTFL  387
HYAL1   ESCQAIKEYMDTTLGPFILNVTSGALLCSQALCSGHGRCVRRTSHPKALL  380


HYAL2   HLSTNSFRLVPGHAPGEPQLRPVGELSWADIDHLQTHFRCQCYLGWSGEQ  437
HYAL1   LLNPASFSIQLTPGGGPLSLR--GALSLEDQAQMAVEFKCRCYPGWQAPW  428


HYAL2   CQWDHRQAAGGASEAWAGSHLTSLLALAALAFTWTL  473
HYAL1   CE---------RKSMW---  435
```

Figure 3. 2 Alignment of HYAL2 and HYAL1.

The human HYAL1, HYAL2, HYAL3, HYAL4, and SPAM1 protein sequences were aligned using ClustalW 2.1. After removing all but the HYAL1 and HYAL2 sequences, gaps that were not required to align HYAL1 and HYAL2 were closed. The sequences used for modeling the protein structures are shown in bold, and strikethrough denotes amino acids excluded from the model. The K148/K144 and P250/P244 residues are shown in red. Residues identified to be important in substrate binding or catalysis using experimental

approaches[13] are indicated in green if they are identical in both proteins and blue if they are conserved.
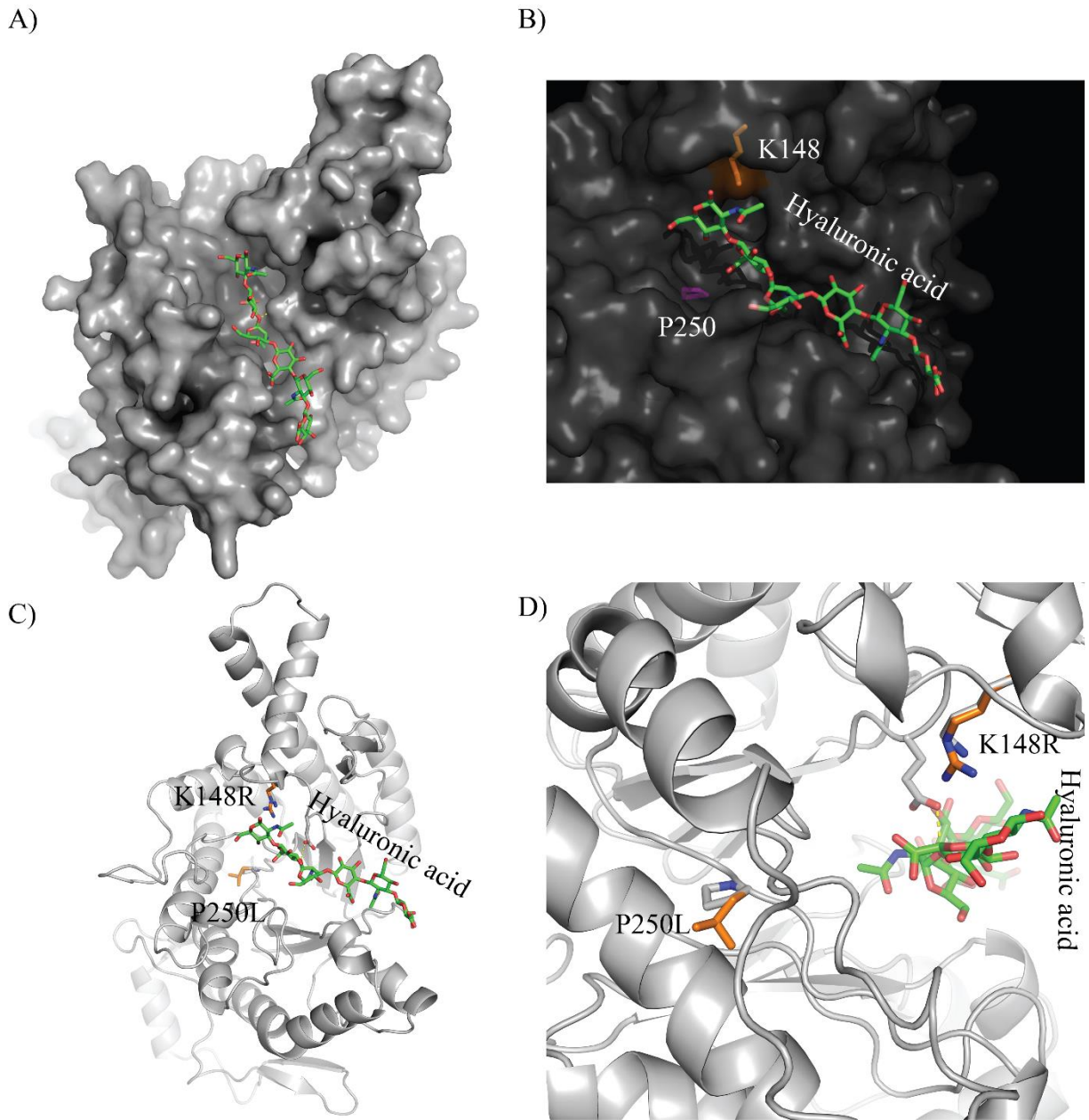
Figure 3. 3 The predicted structure of human HYAL2 bound with its substrate, an HA hexamer.
A) HYAL2 model surface representation (in grey) showing the binding groove with the HA hexamer in stick format, green carbons. B) Enlargement of the surface structure of HYAL2 showing the position of the two amino acid mutations K148 and P250 (shown in stick format (K148 orange carbons and P250 purple carbons). C) Cartoon format showing the structure of HYAL2 bound with HA hexamer. D) Enlargement of the cartoon structure of HYAL2 shows the

position of the wild-type (in grey) and mutated (in orange) residues respectively. The position of K148 appears to be in close proximity to the HA binding site while the P250 residue is deeply buried in the core of HYAL2.

3.4 Generation of expression vectors

To assess the effect of these amino acid substitutions on protein expression, we introduced the mutations into the HYAL2 cDNA that had previously been inserted into the pCMV6-XL5 expression vector. This was done using the fusion strategy shown in Fig. 3.4 where primers containing the single nucleotide changes (corresponding to the c.443A>G; p.K148R and c.749C>T; p.250L mutations) in HYAL2 were used in combination with upstream and downstream primers to generate two PCR products, each bearing the mutation. The two PCR products were then separated by agarose gel electrophoresis and isolated using a gel extraction kit. Following isolation, the two amplified products were used as a template for a fusion PCR using only the outermost primers. The resulting fusion product served as the source for subsequent cloning of the mutation into the *HYAL2* expression vector. To make the full-length construct containing each of the two mutations, the central coding region of HYAL2 within the pCMV6-XL5 vector was removed and replaced with the same region generated from the fusion PCR product using the strategy shown in Fig. 3.4. Both the vector and the PCR product were digested with EcoRI and ApaI, the products were gel purified, ligated and transformed into electrocompetent *E. coli DH5α* by electroporation. After overnight incubation at 37ºC, colonies were picked and grown overnight in 3 ml of LBA.
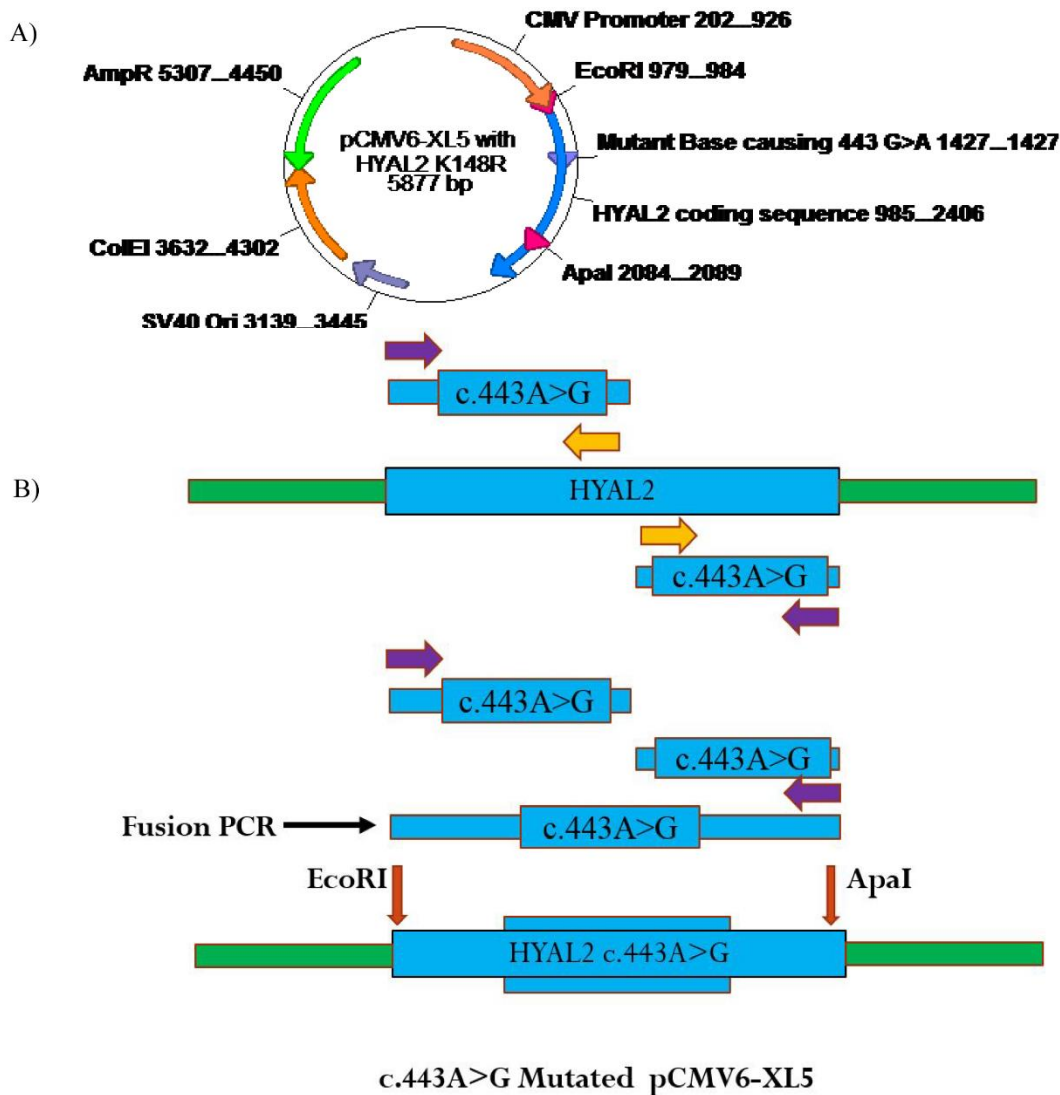
Figure 3. 4 Construction of the HYAL2 expression vector for the K148R HYAL2 mutation.
A) A commercial vector pCMV6-XL5 containing the *Hyal2* sequence within the multiple cloning sites was used as the template. B), The c.443A>G mutation was introduced using primer pairs (shown in yellow) with the c.443A>G nucleotide change for p.K148R in combination with the outer primers (shown in purple) for PCR amplification of the plasmid. Fusion PCR was done using the products isolated from the gel as a template and the outer primers. Finally, the c.443A>G mutation was introduced into the full-length vector by restriction digestion of both the original vector and the fusion PCR amplicon product with EcoRI and ApaI, followed by ligation.

Plasmids were isolated and confirmed to have the desired insert by digestion with EcoRI and ApaI restriction endonucleases, followed by separation by gel electrophoresis (Fig. 3.5). As a final step of confirmation, sequencing was done to ensure that only the desired mutation in the HYAL2 cDNA was present. Finally, the clones were grown in large volume for large-scale preparation of plasmid DNA for transfection.
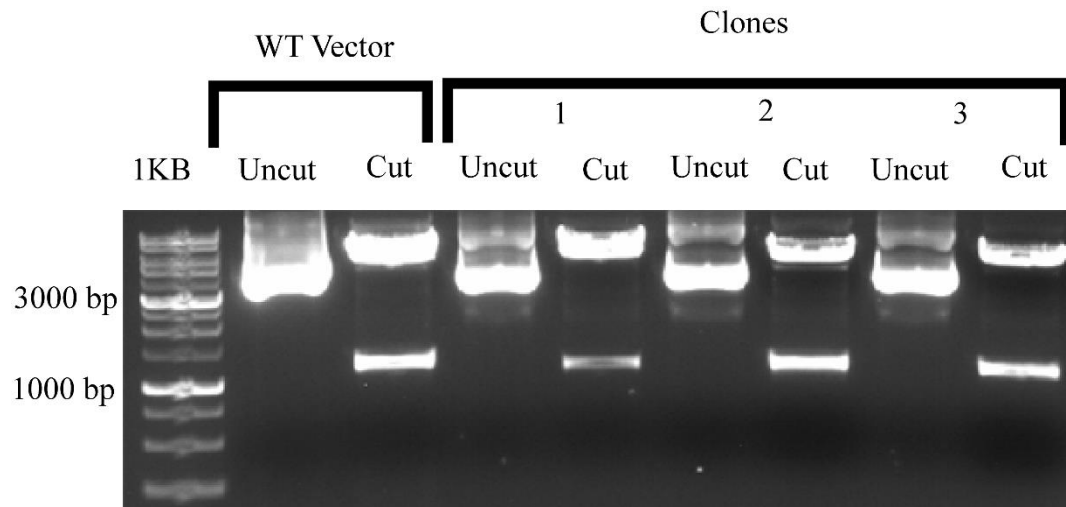
Figure 3. 5 Restriction enzyme analysis of the mutated *HYAL2* plasmids

Uncut or EcoRI/ApaI (Cut) DNA samples were separated on a 1.0 % agarose gel, stained with ethidium bromide and visualized. The expected sizes of the restriction fragments are 4772 bp and 1105 bp. The vector containing the wild-type (WT) HYAL2 cDNA was run to verify the size of the inserted DNA and the fidelity of the insertion. The 1 Kb DNA ladder is shown on the right of the gel.

3.5 Expression of HYAL2-K148R and HYAL2-P250L

To determine if the K148R and P250L mutations impacted the stability of the HYAL2 protein, we co-transfected HYAL2-deficient MEFs with pRc/CMV-β-gal and the *Hyal2* mutation-containing plasmids. Protein levels present in the transfected cell lysates were measured, and β-galactosidase activity was used to adjust the protein concentration within the cell lysates for SDS-PAGE. The approximate level of HYAL2 in the transfection lysates was evaluated by western blot analysis using anti-HYAL2 antibody (Fig. 3.6). Both the K148R and P250L substitutions destabilized HYAL2, resulting in only a low level of HYAL2 that could be detected. When these signals were quantified, the K148R and P250L-HYAL2 had ~20% and ~11% of WT protein levels respectively.
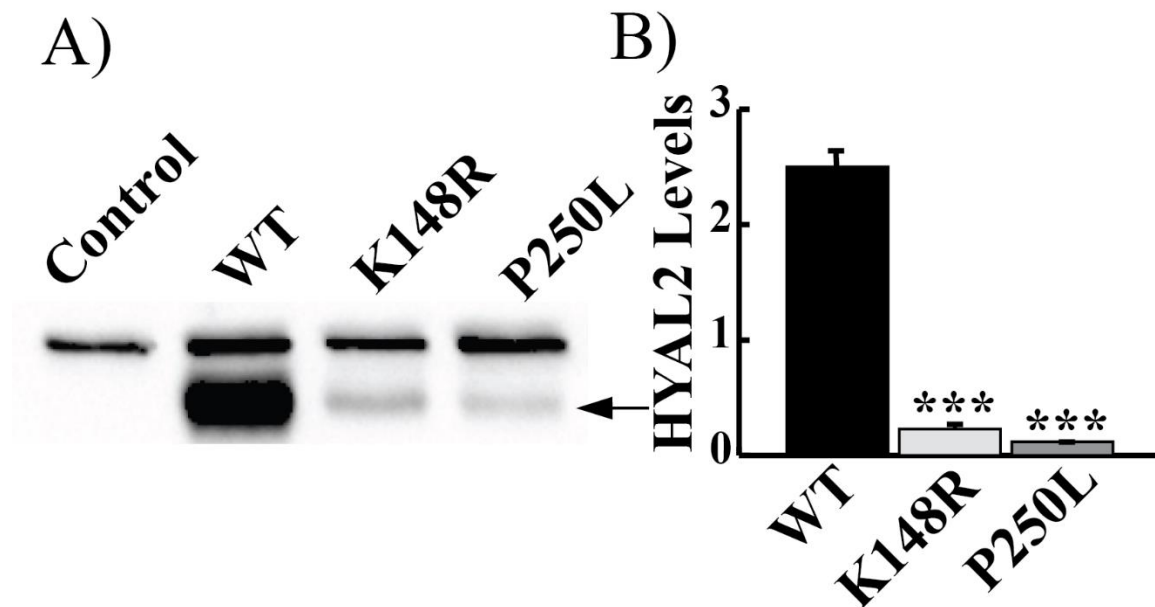
Figure 3. 6 Expression of the mutated HYAL2

A) Western blot analysis of wild-type (WT), K148R- and P250L-HYAL2 expressed in HYAL2 deficient MEFs. Equal levels of β-galactosidase activity were loaded on the gel. The first lane is the control which was transfected with a vector containing a deletion within the HYAL2 starting sequence which prevents the expression of the HYAL2 protein. The black arrow indicates the HYAL2 protein. B) The average level of HYAL2 in the WT and mutant transfection lysates. The columns represent the average level (x 10^6 light units) of HYAL2 ± SEM (n = 4). Significance was determined using the student's T-test and comparing the mutant to the WT vectors. *** indicates p<0.001.

3.6 HA binding assay

From the comparative modeling of the HYAL2 structure bound with the HA hexamer we observed that the amino acid at the 148 position of HYAL2 was located very close to the HA binding site and therefore, a mutation at this residue might affect the binding of the complex with HA for cleavage. To assess the binding of HA with K148R-HYAL2 and WT-HYAL2, we added equivalent amounts of exogenous HA to lysates containing the mutated and wild-type protein that were normalized based on transfection efficiency (β-galactosidase activity). These were allowed to incubate overnight at 4°C to allow binding of HA. Later, the HA bound HYAL2 were precipitated with CPC which is a cationic detergent that has an affinity for anionic HA. The precipitated HYAL2 was then detected with an anti-HYAL2 antibody. The levels of HYAL2 that were precipitated from the expression lysates using HA were similar to the initial levels of HYAL2 in WT and K148R lysates, suggesting no difference in binding HA. The overall expression and signal from the HYAL2 K148R-HA complex are reduced as this reflects the reduced stability of HYAL2 and the smaller band below the full-length protein is likely to be a degradation product (Fig.3.7).
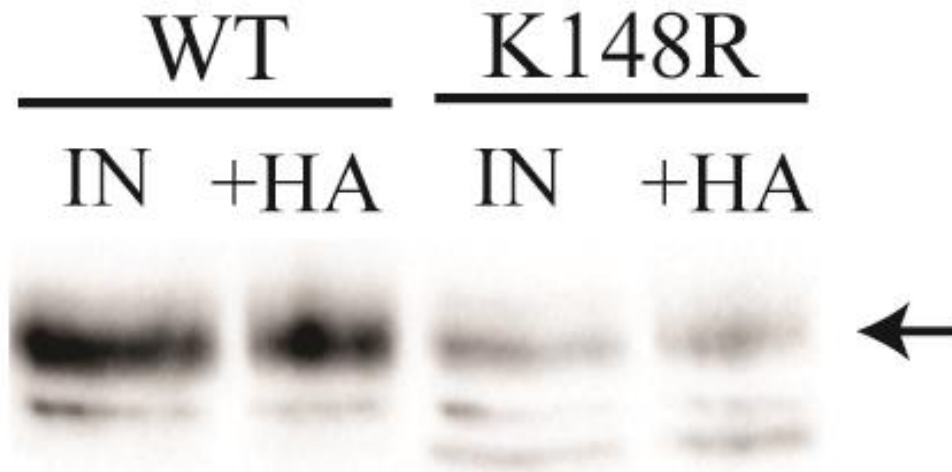
Figure 3. 7 Binding of HA with the WT and K148R-HYAL2.

Western blot analysis comparing initial input (IN) levels of WT and K148R-HYAL2 compared to HA bound HYAL2 (+HA). In both cases, the input levels of HYAL2 are comparable to that brought down with HA. The levels of input protein were normalized to transfection efficiency and are not expected to be equal because of the decreased stability of the HYAL2 K148R protein. The arrow indicates HYAL2 in the gel.

3.7 Hyaluronidase activity assay

Unfortunately, no reliable measurement for HYAL2 enzymatic activity is available at this time. Hence, we decided to model the HYAL2 p.K148R mutation by introducing the equivalent missense mutation (p.K144R) into HYAL1, for which robust methods are available to assay its activity. HYAL1 and HYAL2 have very high sequence identity, and homology modeling of HYAL2 based on the HYAL1 (PDB: 2PE4) structure showed high conservation in the active site. Therefore, we assumed that the changes in the active site of HYAL2 would have a similar impact on HYAL1. To assess the effect of the mutation on the HYAL1 activity, WT and HYAL1 K144R mutants were transiently expressed in the MEFs deficient in HYAL1. Later, WT and mutant HYAL1 expression levels and secretion were assayed by western blotting from the cell lysates and media. The stability of HYAL1 did not appear to be impacted as similar levels of WT and mutant protein were detected in both the cellular lysate and media (Fig. 3.8a). However, using zymography, the level of activity associated with the mutated form of HYAL1 was substantially reduced (Fig. 3.8b). A modified Reissig acid assay was done to quantify the hyaluronidase activity[14]. Although a significant level of activity was detected in both the WT and mutated (K144R) HYAL1, the activity of the secreted K144R HYAL1 was reduced to ~50% of the level that was observed with the wild-type enzyme (Fig 3.8C and Table 3.2).

Table 3. 2 Reissig assay of HYAL1 K144R

Plasmid	Replicate 1			Replicate 2			Replicate 3		
	Average	Normalized	%	Average	Normalized	%	Average	Normalized	%
Control	0.0	0.0	0.0	0.0	0.0	0.0	0.0	0.0	0.0
WT HYAL1	0.063	0.065	100	0.043	0.043	100	0.087	0.087	100
K144R HYAL1	0.033	0.035	55	0.022	0.022	51	0.042	0.042	47.83
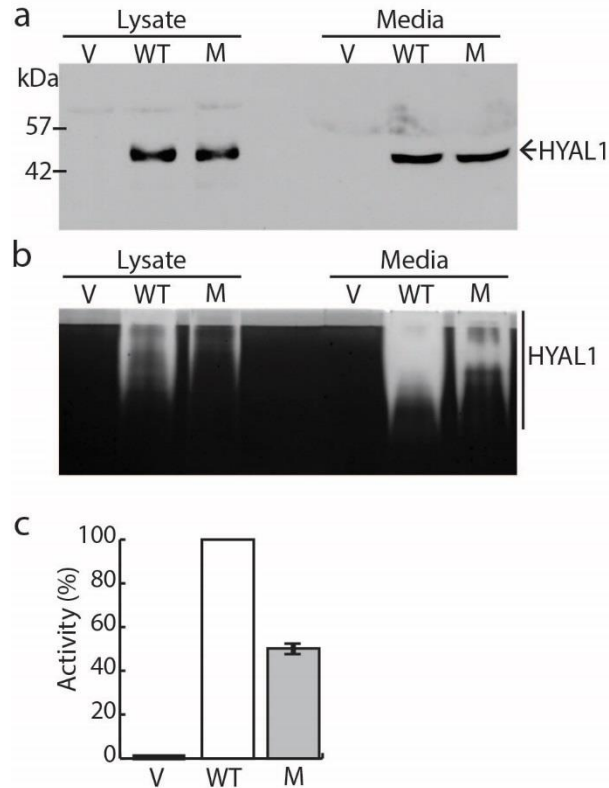
Figure 3. 8 Effect of K144R (K148R equivalent) on HYAL1 activity.

A) Western blot analysis of transiently transfected HYAL1-deficient fibroblasts showed similar levels of WT and K144R-containing HYAL1 in cell lysates. HYAL1 indicated by the arrow. B) Zymography of lysates and media from transfected cells. HYAL1 activity is indicated by the extent of the clearing of the gel (represented by the bright part of the gel). Its migration through this non-denaturing gel is likely as a smear because of interactions with other proteins. C) Quantification of the hyaluronidase activity in the media of transfected cells.

Chapter 4: Results II

Characterization of the developing palate in *Hyal2+/+* and *Hyal2-/-* mice

4.1 Introduction

Mice deficient in HYAL2 were reported in earlier studies to have craniofacial abnormalities[41]. Phenotypically these mice had a broad nose with an increased interorbital distance and an extra bony structure in the suture between the frontal and nasal bones. The identification of cleft lip and/or palate in patients with HYAL2 deficiency led us to further examine the palate phenotype in our mice. Our laboratory showed pre-weaning lethality in 2/3 of the *Hyal2-/-* mice. The *Hyal2-/-* mice also had craniofacial abnormalities similar to that in patients with HYAL2 deficiency, including but not limited to the submucosal cleft palate and increased interorbital distance[44]. MicroCT and H & E staining comparing the palates of postnatal *Hyal2-/-* and *Hyal2+/+* mice showed underdeveloped vomer and ethmoid bones, as well as reduced ossification of the central viscerocranial bones. To further characterize the origin of these abnormalities, we performed histological analyses of the developing palate in mouse embryos collected between E14.5 and E19.5.

4.2 Palate morphology in *Hyal2-/- embryos*

To assess palate structure and morphology, serial paraffin sections from HYAL2 deficient and control embryos were H & E stained. At E13-14, the shelves that will eventually form the palate rapidly grow in the vertical and then horizontal direction as the tongue drops. In embryos collected at these stages, there were no obvious abnormalities in *Hyal2-/-* embryos, but the number of embryos suitable for examination was too small, and the time of collection too variable, to conclude that the growth is normal.

At E15.5, 3 sets of *Hyal2-/-* and control embryos were available for comparison after H & E staining. At this stage, the palate shelves have fused, and condensations of mesenchymal cells

69

are forming and beginning to differentiate in the pattern of the future bones and teeth. The overall morphology of the palate was found to be normal except for the presence of increased matrix in several parts of the viscerocranium. This was indicated by increased space between cells (Fig. 4.1 and 4.3). However, the condensations that will form the maxilla and vomer were decreased in sized and less well defined in *Hyal2-/-* compared to the *Hyal2+/+ or Hyal2+/-* embryos. Similar observations in the middle and posterior palate at E15.5 showed differences in the condensation of the future palate shelf bones in the Hyal2-/- embryos (Fig. 4.1). To further confirm the difference in the developing bone, immunohistochemistry of the anterior palate at 3 pair of E15.5 was done to detect osterix (OSX). OSX is a transcription factor required for osteoblast differentiation and bone formation[145]. OSX levels appeared to be reduced, and the position of the positive cells less defined, in the *Hyal2-/-* compared to wild-type embryos (Fig. 4.2). This area of condensation is in the position of the developing vomer bone, which fuses to surrounding bones of the palate shelf to provide stability and protect the vomeronasal organ.
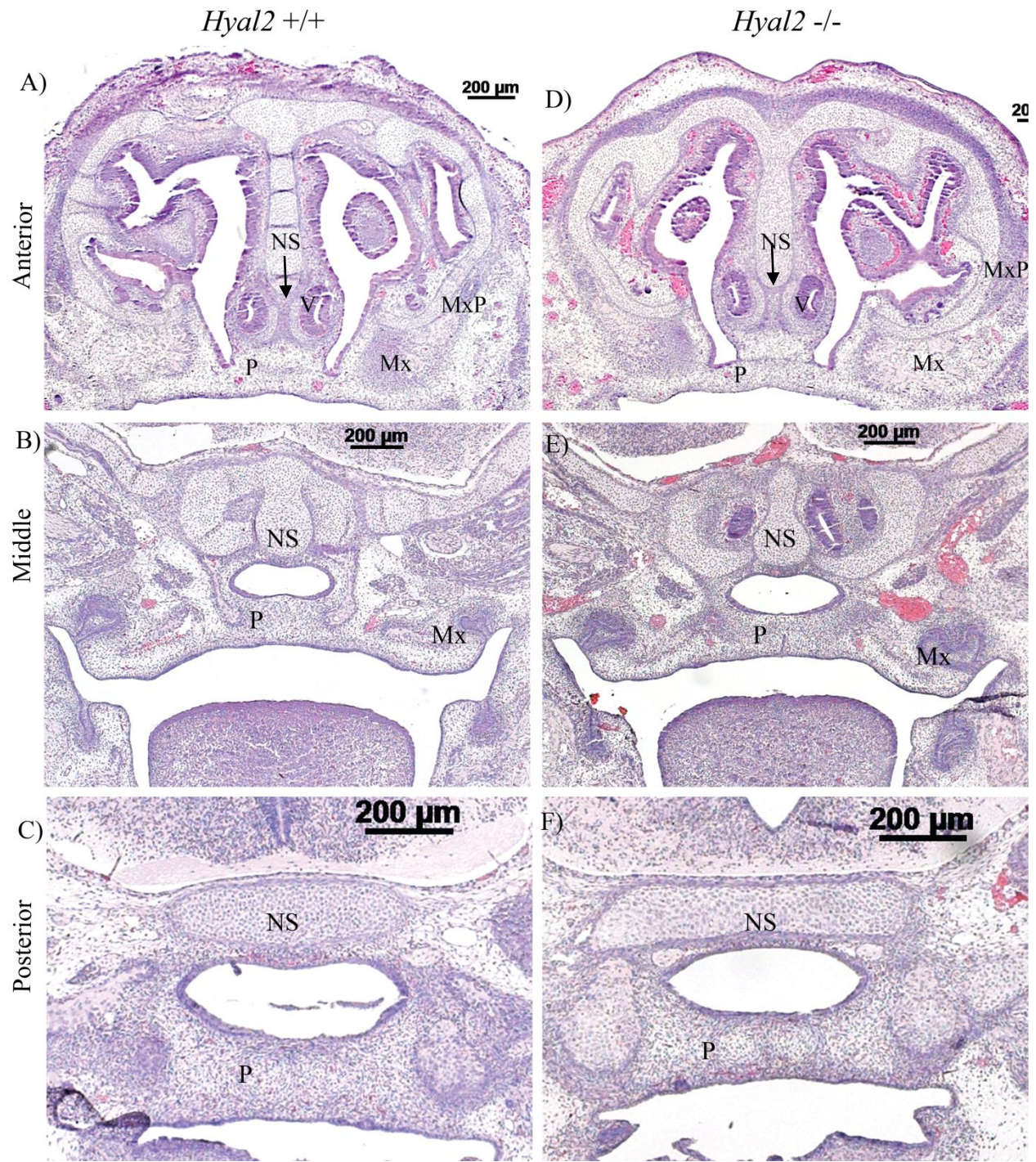
Figure 4. 1 H&E staining of coronal sections from E15.5 embryo palates

A) Anterior palate from *Hyal2+/+* and *Hyal2-/-* embryos. The black arrows indicate areas of reduced vomer bone formation in Hyal2-/- palate B) Middle palate from *Hyal2+/+* and *Hyal2-/-*

embryos C) H&E of the posterior palate from *Hyal2+/+* and *Hyal2-/-* embryos. 3 pairs of *Hyal2+/+* and *Hyal2-/-* embryos were used in this experiment. Scale bars are shown as 200µm (50X). NS= Nasal septum, P=Palate shelf, MxP= Maxillary process, Mx= Maxilla, V= Vomer.
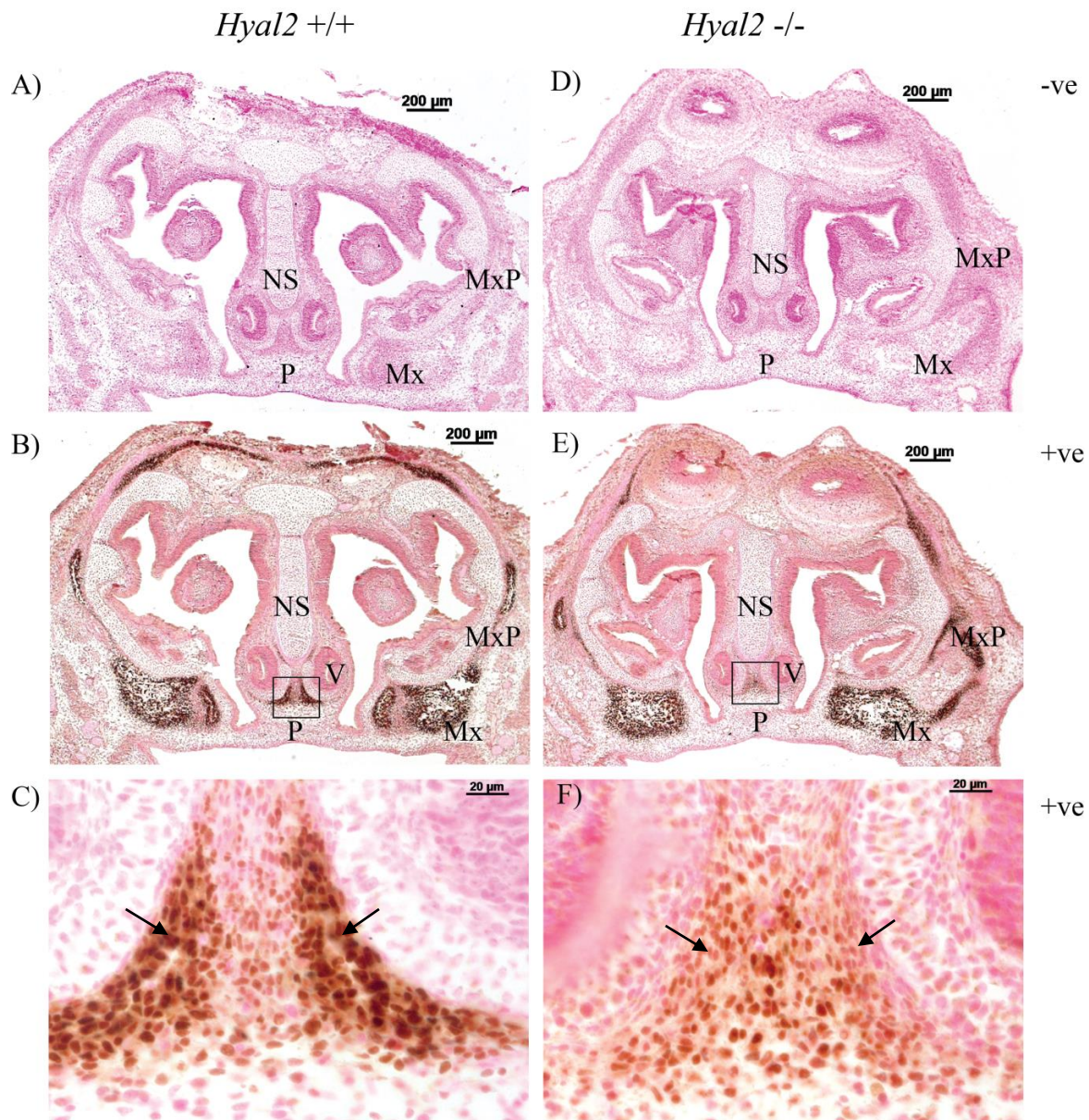
Figure 4. 2 Detection of OSX in the primary palate of E15.5 embryos.

A) Negative controls detected with secondary antibody alone B) Detection of OSX in *Hyal2+/+*

and *Hyal2-/-* embryos. Reduced expression of OSX is evident in the cartilaginous nasal septum

C) Higher magnification of the nasal septum cartilage (shown in the box from B). Arrows

indicate areas of less condensation of the osteoblasts in the *Hyal2-/-* embryos. -ve= negative,

+ve=positive. NS= Nasal septum, P=Palate shelf, MxP= Maxillary process, Mx= Maxilla, V=

Vomer. Scale bars are shown as 200µm (50X) and higher magnification 20µm (200X).

Given that the primary impact of HYAL2 deficiency appeared to be limited to the development of the bone, we chose to examine palate shelf morphology in later stage embryos (E18.5-19.5), after the completion of the palate shelf fusion and growth. Consistent with the earlier embryonic stages, no major changes in morphology were observed, although reduced bone formation was even more apparent in the *Hyal2-/-* embryos when compared to the *Hyal2+/+* embryos (Fig. 4.3). Underdeveloped bones with less fusion to their neighboring bones were evident at all positions within the palate. In addition, reduced condensation of the chondrocytes in the nasal septum was apparent. OSX immunohistochemistry from 3 pairs of E19.5 embryos suggested decreased condensation of osteoblast cells in the cartilage of the nasal septum and palate in *Hyal2-/-* embryos, but this was less dramatic than that seen in the primary palate at E15.5 (Fig. 4.4). These data are consistent with the previous data describing underdeveloped viscerocranium bones in *Hyal2-/-* mice[44].
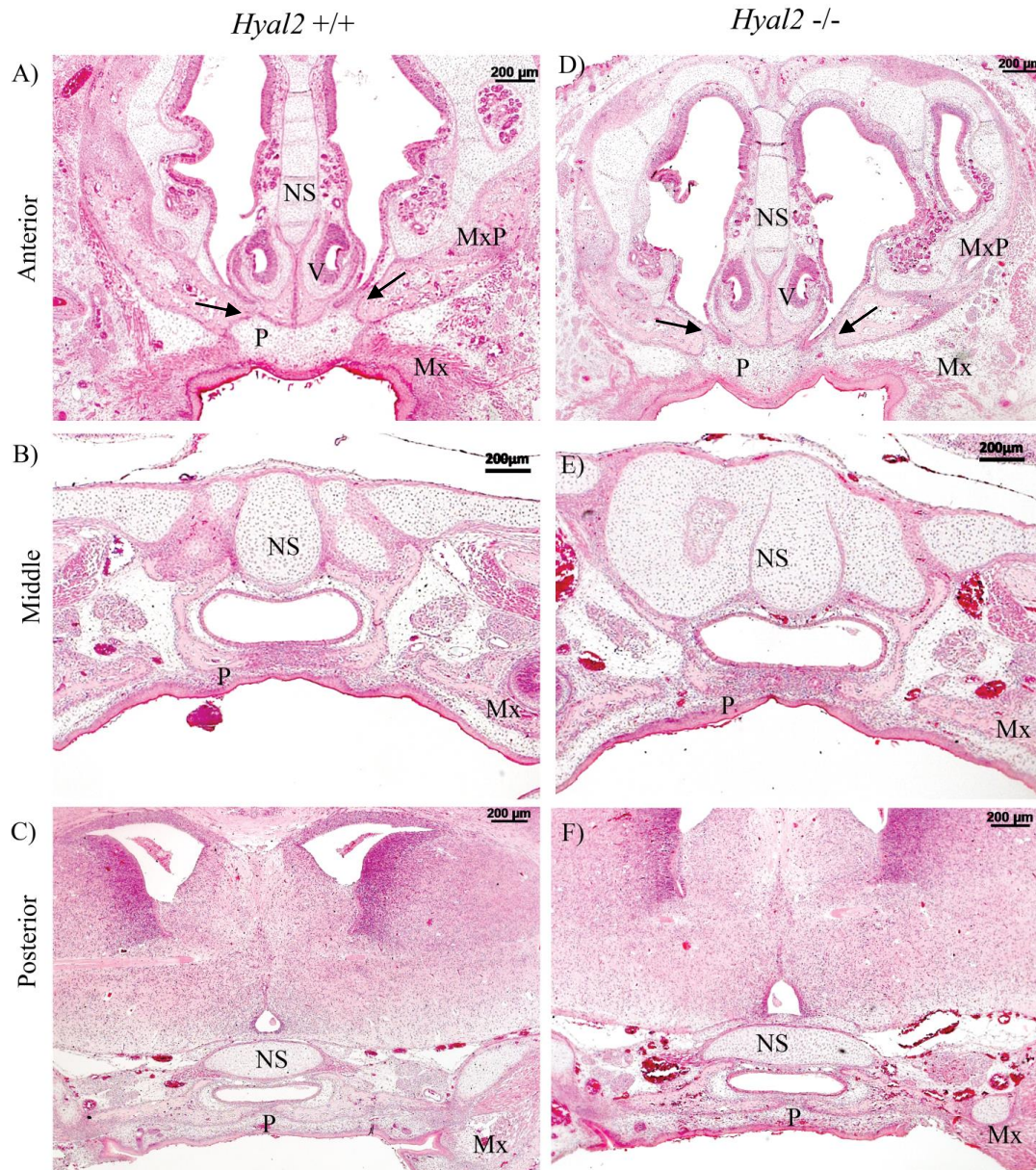
Figure 4. 3 H & E staining of coronal sections from mouse E18.5 palates.

A) and D) Anterior palate of *Hyal2+/+* and *Hyal2-/-* embryos, B) and E) Middle palate of *Hyal2+/+* and *Hyal2-/-* embryos C) and F) Posterior palate of *Hyal2+/+* and *Hyal2-/-* embryos. Arrow indicates areas of bone formation that are reduced in the *Hyal2-/-* embryos compared to *Hyal2+/+* embryos. The arrows indicate discontinuation in the fusion of the vomer and maxilla in the *Hyal2-/-* embryos. NS= Nasal septum, P=Palate shelf, MxP= Maxillary process, Mx= Maxilla, V= Vomer. Scale bars are shown as 200 µm (50X).
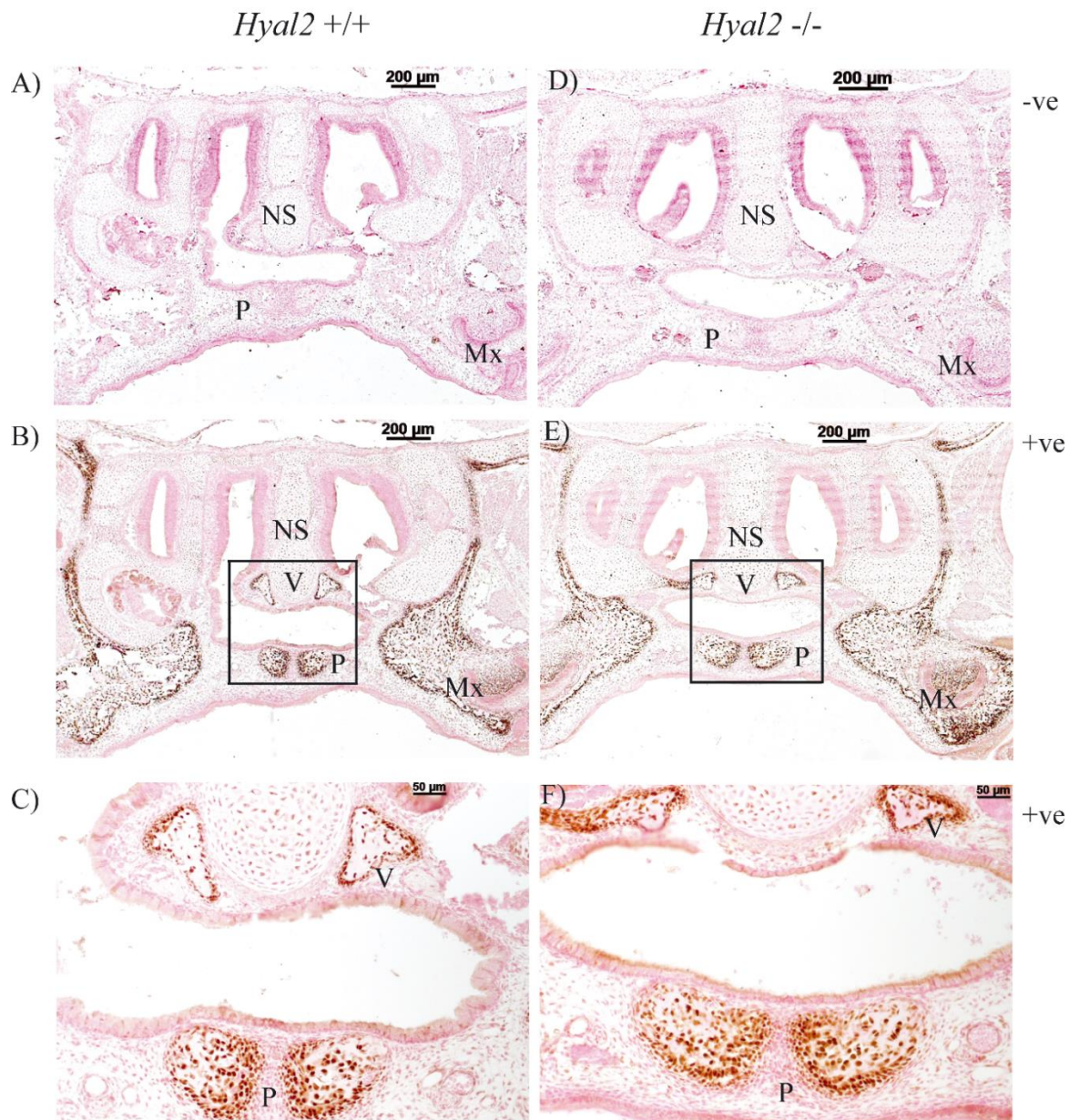
Figure 4. 4 Detection of OSX in the secondary palate of E19.5 embryos.

A) and D) Secondary antibody alone negative control. B) and E) OSX in *Hyal2+/+* and *Hyal2-/-* palates. Reduced expression of OSX is apparent in the bones of the nasopharynx and the secondary palate of *Hyal2-/-* embryos C) and F) Higher magnification of the vomer and palatine bones (shown in the box from B). NS= Nasal septum, P=Palate shelf, MxP= Maxillary process, Mx= Maxilla, V= Vomer, -ve= negative, +ve=positive. Scale bars are shown as 200 µm (50X) and higher magnification 50 µm (200X).

4.3 Bone formation and matrix mineralization

To further characterize the bone formation and mineralization of the palate in the *Hyal2-/-* mouse, alkaline phosphatase (ALP) staining was done on the 3 sets of E19.5 tissues (Fig. 4.5). Both chondryocytes and osteoblasts produce ALP which is known to be required for matrix maturation during osteoblast differentiation[146]. At E19.5 the level of ALP appeared to be higher in the chondryocytes of the nasal septum, but ALP positive bone appeared to be reduced in the palate bones of the *Hyal2-/-* mouse compared to the *Hyal2+/+*consistent with the previous H & E staining and OSX detection. In Fig. 4.5, there is also no fusion of the nasal septum of the *Hyal2-/-* mouse with the epithelial surface of the palate shelf, consistent with the previous description of reduced fusion of the nasal septum surface with the palate[44].

To examine the level of HA in the ECM of the palate of *Hyal2-/-* embryos, histochemistry with HABP was performed on 3 pair of E18.5 sections. An overall increase in detectable HA was found in the matrix of the palate shelf in the *Hyal2-/-* embryos compared to controls (Fig. 4.6).
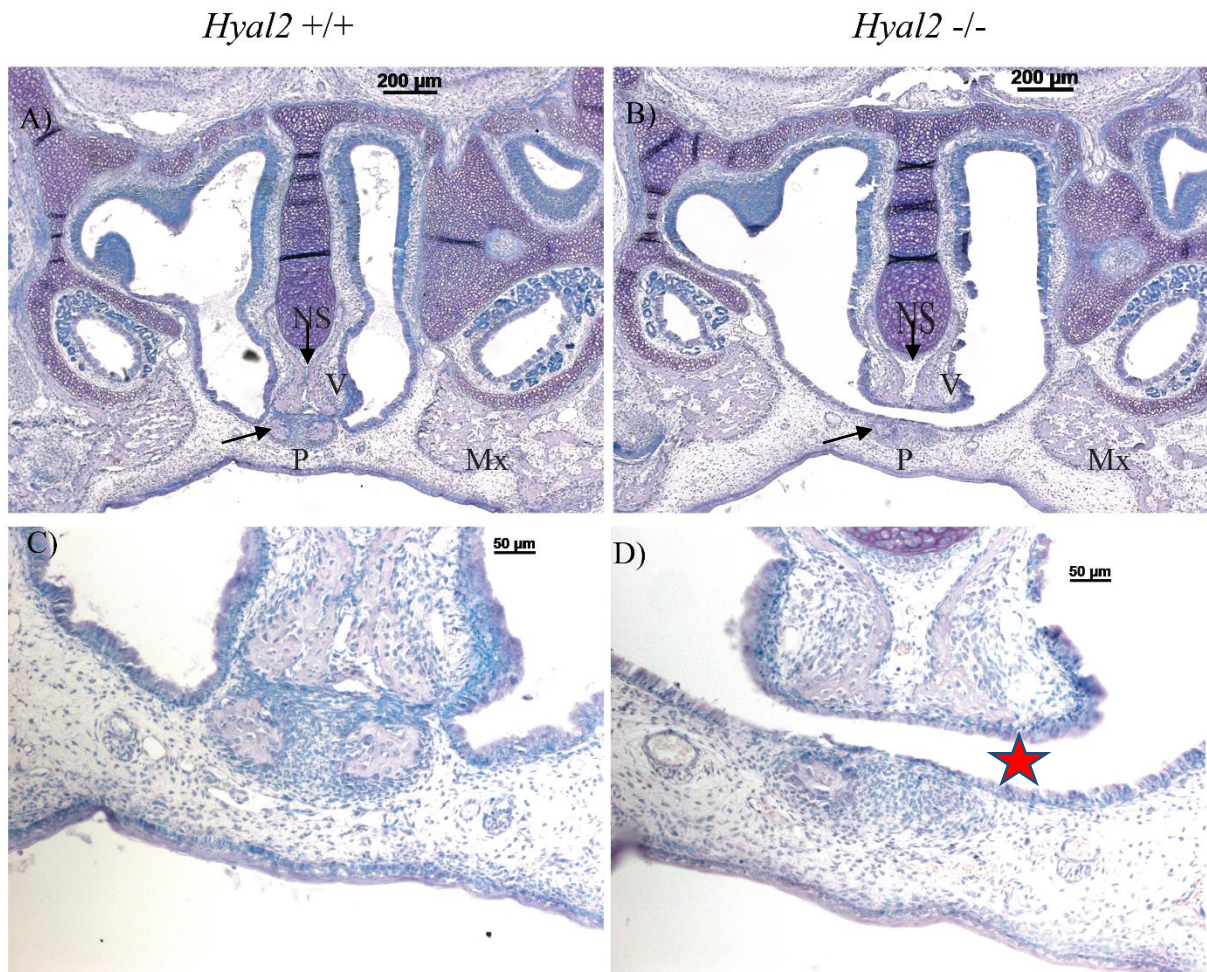
Figure 4. 5 ALP staining of palates from E18.5 embryos.

A) and B) ALP staining of the secondary palate of *Hyal2+/+* and *Hyal2-/-* embryos. The ALP is more abundant in chondrocytes of the nasal septum but lower in regions of underdeveloped bone. Arrows indicate ALP staining in the vomer and palatine bones. C) and D) Enlargement of the area showing the failed fusion in the *Hyal2^{-/-}* embryo (indicated by red star). NS= Nasal septum, P=Palate shelf, Mx= Maxilla, V= Vomer. Scale bars are shown as 200 µm (50X).
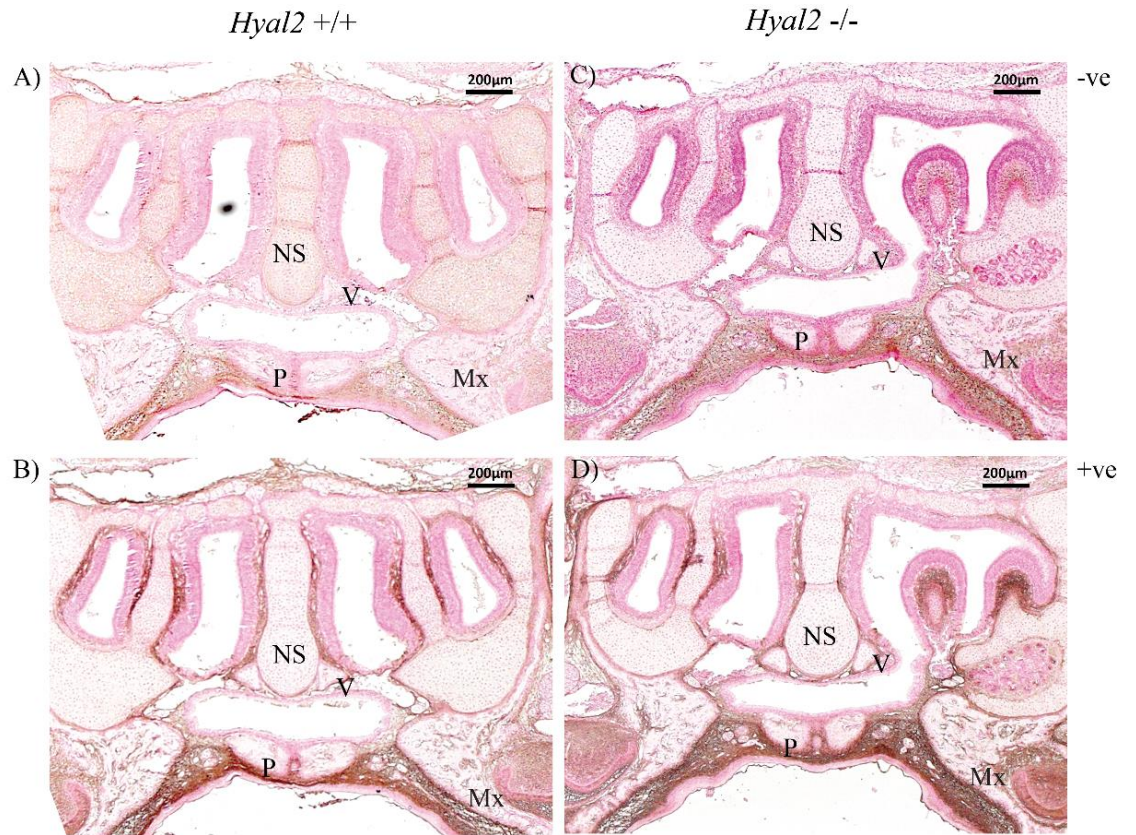
Figure 4. 6 Detection of HA in the palate of the E18.5 embryos

A) and C) Control slides where sections were treated with exogenous hyaluronidase. B) and D) Experimental slides detecting HA with the HABP. *Hyal2-/-* have a slight increase in the extent of matrix that is stained for HA (brown) in the palatal mesenchyme compared to the *Hyal2+/+* embryos. NS= Nasal septum, P=Palate shelf, Mx= Maxilla, V= Vomer. −ve= negative, +ve= positive. Scale bars are shown as 200 µm (50X).

To further characterize the components of the palate of the embryos, we examined periostin distribution. Periostin is a protein secreted by fibroblasts, and its distribution was previously shown to mirror that of collagen I in the palate[147]. Periostin has also been suggested to have a role in osteoblast differentiation[148,149]. We found that periostin was widely distributed and highly expressed in *Hyal2-/-* embryos compared to the *Hyal2+/+* mice (Fig. 4.7). It was consistent with the increased matrix in the *Hyal2-/-* tissues and suggests the presence of a higher level of fibroblasts in the palate.
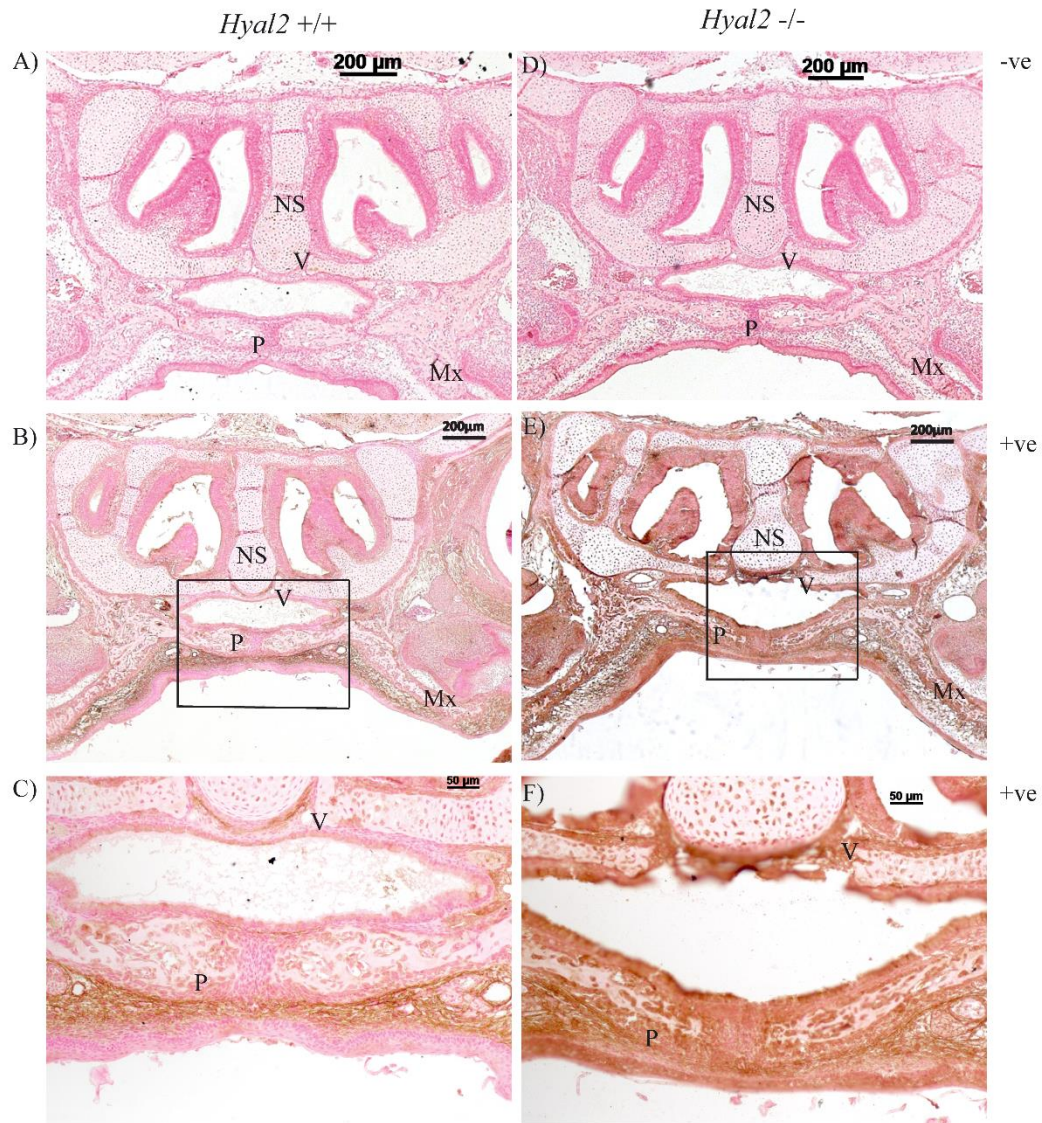
A) and C) Secondary antibody only B) and D) Detection of periostin in *Hyal2+/+* and *Hyal2-/-* palates. C) and E) Higher magnification of the secondary palate (shown in the box from B). . NS= Nasal septum, P=Palate shelf, Mx= Maxilla, V= Vomer. −ve= negative, +ve= positive. Scale bars are shown as 200 µm (50X) and higher magnification 50 µm (200X).

4.4 EMT gene expression analysis

The increased level of periostin in the palate suggests fibroblastic cells are higher in the HYAL2 deficient mouse and higher level of the HA accumulation in the ECM in the *Hyal2-/-* mouse might interfere with the EMT process during embryonic development. To determine how HYAL2 deficiency might affect signaling pathways involved in EMT and HA metabolism, we analyzed the expression levels or of 42 genes in these pathways and 3 housekeeping genes. All assays were done with PrimeTime® gene expression assays purchased from IDT with a guaranteed amplification efficiency >95%. RNA isolated from E12.5 Hyal*2-/-* and *Hyal2+/+* nasopharynx tissues were used for reverse transcription. Samples prepared with and without reverse transcriptase were used to determine the level of expression of these genes using qPCR. Results from two independent biological replicates (n=2) are shown in Fig. 4. 10. Although there was considerable variability between the replicates, most of the EMT genes in this array appeared to be downregulated (FC >1.0). Downregulation in *Col1a2* expression suggests a reduction in the maturation of cartilage which is consistent with the decreased condensation observed in the nasal septum of the *Hyal2-/-* embryos. The most dramatic impact was on *Hyal1* expression, which was increased 2.5-fold in the *Hyal2-/-* sample which suggests HYAL1 might be increasing to degrade accumulating HA. Reduction in the *Sox10* expression, a marker of NCCs, was surprising as opposite findings were found in studies of the heart in our lab (unpublished data). The decreased *Sox10* expression may suggest a decreased number of neural crest derived cells in the sample that was analyzed. This could reflect a bias in sample collection where more neural tissue was included in the wild type that then knockout sample. Further studies using more carefully dissected tissues will be needed to further assess these findings.
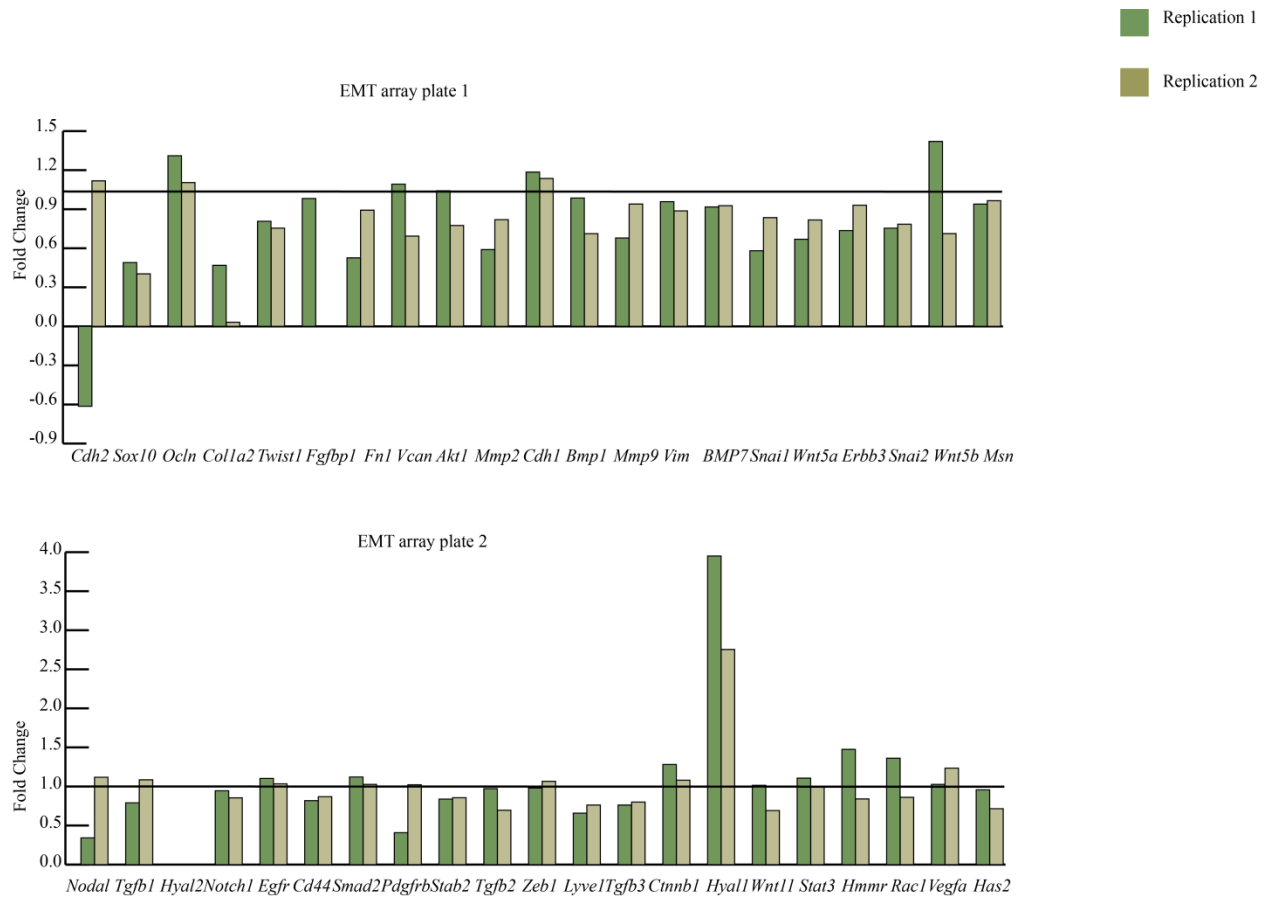
Figure 4. 8 Expression of 42 genes involved in EMT or HA metabolism.

The bar graph shows the fold change in the expression of 42 genes in *Hyal2-/-* compared to *Hyal2+/+* tissues in two biological replicates. Genes with FC level <1.0 are down-regulated. The two different shades of green color represent result from two independent replicates.

Chapter 5: Discussion and conclusion

5.1 Discussion and conclusion

HA is a major component of the vertebrate ECM and undergoes turnover and degradation in normal and different pathological states[52]. HA degradation has been reported to be catalyzed primarily by HYAL1 and HYAL2. It is proposed that HA degradation initially starts with the action of HYAL2, which is a GPI-anchored protein attached to the plasma membrane, and is later continued in the lysosome through the action of HYAL1 and exoglycosidases[30]. In addition to maintaining normal tissue homeostasis, HA also plays a significant regulatory role during vertebrate development.

The importance of HA in embryonic development has been characterized by the studies of HAS2 deficient embryos. HAS2 KO embryos failed to develop normal cardiac cushions and died at E9.5 due to the failure of EMT of the cardiac endothelial cells[150]. A role for HYAL2 in somatic HA degradation has been demonstrated in previous studies showing accumulation of HMM-HA in various tissues in HYAL2 deficient mice[42]. Characterization of HYAL2 KO mice revealed craniofacial abnormalities, cardiac dysfunction, hearing loss, renal agenesis and mild anemia which indicated HYAL2 had a role in the regulation of HA homeostasis during organ development[41,44]. Patients with mutated forms of HYAL2 also shared similar abnormalities affecting the facial bones and heart pathologies as well as hearing loss and myopia[44]. Characterizing the effects of HYAL2 K148R and P250L through functional studies we found that HYAL2 mutations reduces the level of protein expression and caused HYAL2 deficiency. Further, qualitatively analyzing the morphology and histology using some markers of bone development in the developing palate of HYAL2 deficient embryos, we found poor palatal bone formation compared to the controls. Earlier studies indicated that bone development might be spatially and temporally regulated by HA during early development; higher levels of HA might

promote EMT during embryogenesis while it's removal might promote differentiation. These observations are discussed in following sections.

5.1.1 Comparison of the homology model of wild-type and mutated HYAL2

This work started with the functional characterization of the two mutations in HYAL2 (chapter 3) first identified in humans by homozygosity mapping and NGS. Amino acid substitution K148R and P250L were found respectively in the HYAL2 of Amish and Saudi Arabian cohorts with orofacial clefting[44]. The lysine (K) at the 148 position is conserved among HYAL2 homologs, but not in the orthologue HYAL3, or in some more distantly related hyaluronidases. However, homology modeling of HYAL2 showed that the K148 residue falls into the binding site groove of HYAL2, and therefore could impact HYAL2 structural and catalytic integrity. The substitution of the positively charged Lys148 to Arg- a longer side chain containing amino acid might interfere with the shape of the HA binding subsite resulting in compromised binding affinity and substrate catalysis activity of HYAL2. In contrast, Pro250 was found to be interiorly buried in the core of HYAL2. Substitution of the structurally distinct and polar Pro250 to a non-polar Leu residue is speculated to distort overall structure and impact the proper folding of HYAL2. The misfolding of proteins that transit the ER-Golgi pathway typically leads to transport out of the ER and degradation by the proteasome and therefore would not reach the cell surface.

5.1.2 HYAL2 expression, HA- binding and activity

Expression of the mutated forms of HYAL2 in MEFs deficient in HYAL2 showed a significant reduction in HYAL2 levels compared to the wild-type protein. Surprisingly, both amino acids destabilized HYAL2, resulting in low levels of residual protein. It is difficult to know how this compares to the human situation as no tissues appropriate for the analysis of HYAL2 protein were available to us. However, overexpression studies typically result in more residual protein that one would see endogenously, and therefore it is likely that the human patients have a very low level of residual HYAL2 protein. Given that the K148R mutated form of HYAL2 was slightly more stable than the P250L-mutated form, we also assessed the impact of K148R on HA binding and activity. A comparison of the HA binding between the wild-type and the K148R HYAL2 did not reveal any significant difference in overall affinity. There was, however, some degradation product from the K148R HYAL2 that indicated this protein was less stable and susceptible to proteolytic degradation. Without a reliable assay for HYAL2 activity available, we assessed catalytic activity by introducing the equivalent missense mutation (K144R) into HYAL1. Surprising, this mutation had less impact on HYAL1 stability but did significantly decrease its activity. Therefore, it is possible that the residual HYAL2 containing the K148R mutation is also enzymatically less active.

The finding of residual protein after overexpression is consistent with the phenotype of the patients with HYAL2 deficiency. HYAL2 deficiency is lethal in 2/3 of mice, but in humans, the phenotype appears less severe. In mice with complete HYAL2 deficiency, there is more than a 10-fold elevation in circulating HA, whereas there was no increase in circulating HA in the human patients. This may be because there is sufficient residual HYAL2 in the human patients to

degrade HA except in times of very high turnover such as during development. It is possible that a complete deficiency of HYAL2 would also be lethal in humans.

5.1.3 Comparison of palate morphology in *Hyal2+/+* and *Hyal2-/-* embryos

A comparison of the palate morphology started with collection, processing, sectioning and histologic analysis of the palate structure from embryos at E13.5-E19.5 (Chapter 4). H & E staining was done for the assessment of the palate from both the *Hyal2+/+* and *Hyal2-/-* embryos. However, because of variability in the time of collection of early-stage embryos and processing artifacts, only embryos from E15.5 and E18.5 were available for study. At E15.5, 3 sets of HYAL2 deficient and wild-type embryos were compared by H&E staining of the anterior, middle and posterior palate. In comparisons of these sections, no gross difference in the overall palate morphology was identified. However, the presence of excess ECM and less condensation in the areas of developing viscerocranium bones (maxilla, vomer, palatine) was observed in the *Hyal2-/-* embryos compared to the controls (Figure 4.1). Reduced condensation of the bone matrix in the future secondary palate forming areas from the posterior palate also appeared in the *Hyal2-/-* compared to the *Hyal2+/+* embryos. Comparison of the palate morphology from the 3 sets of H & E staining from late-stage E18.5-E19.5 *Hyal2+/+* and *Hyal2-/-* embryos was also consistent with the observations from E15.5. In fact, reduced condensation in bone and cartilage of the secondary palate, vomer, and maxilla was more apparent in the late stages (Figures 4.3 and 4.4).

5.1.4 Comparison of osteoblast formation in *Hyal2+/+* and *Hyal2-/-* embryos

To further validate the characteristics of the bone formation in the palate structure from *Hyal2+/+* and *Hyal2-/-* embryos, we did IHC using anti-OSX antibody (a marker for osteoblast

differentiation and bone development). At E15.5, the detectable OSX in the developing vomer appeared to be reduced, and the positive cells were not defined to a specific region, compared to the wild-type embryos (Fig. 4.2). Similarly, at E19.5 *Hyal2-/-* embryos had less OSX positive osteoblast cells in the secondary palate bone and nasal septum cartilage (Figure 4.4), although the difference was less prominent than that at E15.5. Overall, the reduced bone formation is consistent with that observed in the *Tbx22-/-* mice which have classical SMCP and severely reduced the formation of the vomer and secondary palate bones. *Tbx22-/-* mice have phenotypes of SMCP (sub mucous cleft palate) due to mutation in the T-box 22 gene that encodes a transcription factor. Moreover, consistent with the *Hyal2-/-* embryos reduced ossification (see below) of the craniofacial bones was also evident in the *Tbx22-/-* embryos[151].

5.1.5 Comparison of matrix mineralization and bone formation in *Hyal2+/+* and *Hyal2-/-*

To assess the matrix maturation level and bone formation, ALP staining was done in both the control and *Hyal2-/-* embryos. ALP is secreted by both the chondrocytes and osteoblasts in the developing bone. Although at E19.5, the overall ALP level in the chondrocytes of the nasal septum was comparatively higher, the level in the palate bones of HYAL2 deficient mice appeared reduced (Fig. 4.5). From earlier micro-CT data, the reduced density of the bones is in the most central area of the viscerocranium, indicating a central mineralization defect. This observation is also consistent with the OSX level and H & E staining at E19.5. The central mineralization defect was also observed in previous microCT studies of the viscerocranium at P1 and E18.5[26]

5.1.6 HA accumulation in the matrix of the *Hyal2-/-* embryos

Previous studies have shown that HA accumulated in most tissues of adult HYAL2 deficient mice. Indeed, increased levels of detectable HA were observed in the palates of E18.5 *Hyal2-/-* embryos compared to the controls (Fig. 4.6). Earlier reports from the brachymorphic mice (characterized by "shortening of long bones, dome-shaped skull, and a short thick tail) suggested that HA provides a matrix environment that promotes rapid matrix mineralization in a random fashion[152]. Due to the deficiency in HYAL2, failure to remove HA may result in an excess deposition in the ECM which in turn might interfere with the normal osteoblast differentiation and therefore reduce bone matrix maturation. Although our results are consistent with this concept, further studies would be needed as other interpretations are possible.

HA levels have previously been hypothesized to play a role in normal palate development, but whether increased or decreased levels cause CP has been controversial. Studies with *Sim2-/- mice* showed increased HA levels in the ECM were associated with craniofacial abnormalities while reduced HA was also described as a risk factor for CP in *Tbx1-/-* mouse[153,154]. Reports from in vitro studies involving the role of HA in osteogenic differentiation suggested that MW and concentration of HA regulated bone formation[155]. A requirement for HA removal after condensation of the matrix and osteogenesis of the bone was also reported in vitro studies of mouse intramembranous osteogeneis[156]. Consistent with the earlier in vitro reports our study also suggests a time-specific role for HA during bone development where its presence during early stage is required for mesenchymal cell proliferation but needs to be removed later to allow cells to congregate and mineralize the bones during the process of differentiation. This indicates that HA may play a role in regulating EMT in the developing palate as has been suggested previously in studies of the heart[62].

5.1.7 EMT microarray analysis of the craniofacial area of *Hyal2+/+* and *Hyal2-/-*

We performed two independent replicates of gene expression arrays relevant to EMT and HA metabolism using tissues from the craniofacial area of E12.5 *Hyal2+/+* and *Hyal2-/-* embryos. Our normalized data compared to the *Hyal2+/+* suggested most of the EMT related genes were downregulated in the *Hyal2-/-* except *Hyal1, Cdh1, Cdh2, Wnt5b* and *Vegfa* genes which have higher FC >1 values. Some of the genes (i.e. *Lyve-1*, *Hmmr*) that act as a receptor for HA during degradation are also slightly downregulated. The greatest increase in expression was of *Hyal1* (FC 2.5) indicating that HYAL1 might be responding to altered HA metabolism in *Hyal2-/-* tissues. The downregulated expression of *Sox10* reflects lack of neural crest derived cells in the *Hyal2-/-* tissues. *Sox10* regulates several transcriptional targets involved in maintaining progenitor cell multipotency, speciation and cellular differentiation[157]. Loss-of-function mutations in the *Sox10* gene have been found in patients with Kallmann syndrome[158,159]. Functional analysis of a *Hyal2* mutation Asp236Gly from a Kallman syndrome patient in our lab found reduced level of the HYAL2 when expressed in the MEF cells deficient in HYAL2 (unpublished data). This data along with the underdeveloped vomer bones found in the *Hyal2-/-* mouse suggests *Hyal2* might impact neural crest cell migration because HYAL2 degrades HA to maintain extracellular matrix homeostasis required for cellular migration. Our EMT array data also showed reduced expression of the *Col1a2* a cartilage collagen required for the formation of triple helix of type I collagen for cartilage development. Further confirmation of the expression level of these genes is required to assure their involvement in the developing palate.

Chapter 6: Limitation and future direction

6.1 Limitations of the HYAL2 protein analysis

Transient expression studies might lead to the misinterpretation of the overall result. Protein overexpression in mammalian cell culture could overload the cellular environment and create toxicity by aggregation of the misfolded proteins. impacting the level of protein production, folding and localization[160,161]. Careful consideration is required when interpreting the overexpression studies, and ideally, analysis of the levels of HYAL2 in tissues from the patients is needed. Analysis of the HA binding also suffers from experimental limitations. In this case, exogenous HA is used to bind with HYAL2 extracted from cell lysates. However, HA typically exists in association with other binding proteins, including receptors such as CD44, HARE, and LYVE-1, that may be required prior to the catalysis by HYAL2 in the plasma membrane. The proper environment for HA binding may not be present. Furthermore, we did not make any attempt to test binding to a different amount or molecular size of HA which might reveal differences in affinity that were not evident when the exogenous HA was in excess. One significant weakness in our studies was the absence of an assay to directly examine the enzymatic activity of HYAL2. Studies have described HYAL2 shows weak activity towards its substrate and possibly requires another binding partner for catalysis which has not yet been characterized. Although the advantages of HYAL2 having high sequence identity and similarity of the active site with HYAL1 was taken to assess the impact of the mutated residue on protein activity, this is in fact not the true measurement of HYAL2 function. Comparing all the characteristics and limitations of the in vitro experiments, it is desirable to study both HA and HYAL2 levels in tissues from the human patients.

6.2 Limitations and future direction of the palate study

Due to challenges in tissue processing and sectioning at early embryonic stages, the scope of our study was limited, but future directions would include looking at cell proliferation during early palate development. Increasing the number of samples analyzed at E15.5 and E18.5 would determine if the full palate phenotype associated with HYAL2 deficiency has been examined and provide increased validity to the current conclusions of decreased condensation and bone formation. The EMT microarray from the palate could be repeated, but probably more importantly the area dissected needs to be refined by laser capture microdissection. Reports from the NIH FACEBASE consortium showed differences at E14.5 in the expression of genes even within the palate[162]. Given the variation reported in the levels of gene expression on the nasal and oral side of the anterior and posterior palate, we decided that refinement in the approach to tissue collection be needed. This would be a priority for future studies aimed at fully elucidating how HYAL2 functions in the palate.

These studies definitively demonstrate an important role for HYAL2 in palate development and indicate that a deficiency in HYAL2 can predispose to palate abnormalities.

Appendix 1: List of EMT related genes and their target used in the EMT array experiment.

Gene	Target
Nodal Nodal growth differentiation factor	Regulates gene expression by binding with SMAD family transcription factors
Tgfb1 Transforming growth factor beta 1	Controls proliferation, differentiation, and apoptosis signaling in some cell types.
Notch1 Notch homolog 1	Regulates interactions between physically adjacent cells through binding of Notch family receptors to their cognate ligands.
Egfr	Cellular proliferation
Smad2	Regulates cell growth and proliferation mediating TGF-beta signaling
Pdgfrb platelet derived growth factor subunit B	Activates downstream signaling pathways, inducing cellular proliferation, differentiation, survival, and migration
Tgfb2 Transforming growth factor-beta 2	Regulates gene expression by binding with SMAD family transcription factors
Zeb1 zinc finger E-box binding homeobox 1	Negatively regulates transcription of interleukin 2
Tgfb3 Transforming growth factor-beta 3	Provide signals for palatal seam EMT in mice by influencing the expression of *Lef1*(Lymphoid enhancer binding factor 1)
Ctnnb1 Beta catenin	One of the adherent junction proteins. maintains epithelial cell layers by regulating cell growth and adhesion between cells, anchors the actin cytoskeleton , transmits the contact inhibition signal
Wnt11 Wnt family member 11	Regulates of cell fate and patterning during embryogenesis
Stat3 signal transducer and activator of transcription 3	Mediates the expression of a variety of genes in response cytokine-induced changes and plays a key role in many cellular processes such as cell growth and apoptosis.
Cdh2 cadherin 2	Maintains cell-cell adhesion, development of the nervous system and the formation of cartilage and bone
Akt1 AKT serine/threonine kinase 1	Regulates metabolism, proliferation, cell survival, growth and angiogenesis
Wnt5a Wnt family member 5A	Regulates of cell fate and patterning during embryogenesis
Sox10 SRY-box 10	Influences embryonic development by regulating NCC function
Mmp2 matrix metallopeptidase 2	Degrades ECM, regulates embryonic development and tissue remodeling
Erbb3 erb-b2 receptor tyrosine kinase 3	Signal transduction by encoding a epidermal growth factor receptor
Rac1 ras-related C3 botulinum toxin substrate 1	Controls cell growth by mesenchymal cell migration, neuronal polarization, axonal growth, and differentiation
Ocln occludin	Regulates the maintenance of cellular tight junctions

Gene	Target
Cdh1 cadherin 1	Maintains cell-cell adhesion, development of the nervous system and the formation of cartilage and bone
Snai2 snail family transcriptional repressor 2	Regulates EMT by repressing the expression of E-cadherin
Vegfa vascular endothelial growth factor A	Proliferation and migration of vascular endothelial cells, angiogenesis
Col1a2 collagen type I alpha 2 chain	Provides support for cartilage, bone, tendon, skin
Bmp1 bone morphogenetic protein 1	Induces cartilage formation
Wnt5b Wnt family member 5B	Regulates of cell fate and patterning during embryogenesis
Twist1 twist family bHLH transcription factor 1	Transcription factor functions in cell lineage determination, differentiation
Mmp9 matrix metallopeptidase 9	Degrades ECM, regulates embryonic development and tissue remodeling
Msn Moesin (membrane-organizing extension spike protein)	Function as cross-linkers between plasma membranes and actin-based cytoskeletons
Fgfbp1 fibroblast growth factor binding protein 1	Plays a critical role in cell proliferation, differentiation and migration by binding to fibroblast growth factors and potentiating their biological effects on target cells.
Vim Vimentin	Encodes intermediate filaments, maintains cell shape, integrity of the cytoplasm, and stabilizing cytoskeletal interactions.
Fn1 Fibronectin1	Cell adhesion and migration processes during embryogenesis,
Mmp7 matrix metallopeptidase 7	Degrades ECM, regulates embryonic development and tissue remodeling
Vcan versican	Encodes chondroitin sulfate proteoglycan, involved in cell adhesion, proliferation, proliferation, migration and angiogenesis and plays a central role in tissue morphogenesis and maintenance.
Snai1 snail family transcriptional repressor 1	Regulates EMT by repressing the expression of E-cadherin
Stab2 stabilin 2	Function in angiogenesis, lymphocyte homing, cell adhesion, or receptor scavenging, HA receptor
Hmmr hyaluronan mediated motility receptor	HA receptor, functions in cell motility
Lyve1 lymphatic vessel endothelial hyaluronan receptor 1	HA receptor
Cd44 Cluster of differentiation 44	Involves in maintaining cell-cell interactions, cell adhesion and migration

Reference

1. Rodén, L. *et al.* Enzymic pathways of hyaluronan catabolism. *Ciba Found. Symp.* **143,** 60-76-86, 281–5 (1989).

2. Kreil, G. Hyaluronidases--a group of neglected enzymes. *Protein Science* **4,** 1666–1669 (1995).

3. Pavasant, P., Shizari, T. M. & Underhill, C. B. Distribution of hyaluronan in the epiphysial growth plate: turnover by CD44-expressing osteoprogenitor cells. *J. Cell Sci.* **107 (Pt 1,** 2669–2677 (1994).

4. Duran-Reynals, F. Studies on a certain spreading factor existing in bacteria and its significance for bacterial invasiveness. *J. Exp. Med.* **58,** 161–81 (1933).

5. Stern, R. & Jedrzejas, M. J. Hyaluronidases: Their genomics, structures, and mechanisms of action. *Chemical Reviews* **106,** 818–839 (2006).

6. Csóka, A. B., Scherer, S. W. & Stern, R. *Expression Analysis of Six Paralogous Human Hyaluronidase Genes Clustered on Chromosomes 3p21 and 7q31. Genomics* **60,** (1999).

7. Wei, M.-H. *et al.* Construction of a 600-Kilobase Cosmid Clone Contig and Generation of a Transcriptional Map Surrounding the Lung Cancer Tumor Suppressor Gene (TSG) Locus on Human Chromosome 3p21.3: Progress toward the Isolation of a Lung Cancer TSG. *Cancer Res.* **56,** (1996).

8. Frost, G. I., Csóka, a B., Wong, T. & Stern, R. Purification, cloning, and expression of human plasma hyaluronidase. *Biochem. Biophys. Res. Commun.* **236,** 10–15 (1997).

9. Kim, E. *et al.* Identification of a hyaluronidase, Hyal5, involved in penetration of mouse sperm through cumulus mass. *Proc. Natl. Acad. Sci. U. S. A.* **102,** 18028–18033 (2005).

10. Zhang, H. & Martin- Deleon, P. A. Mouse Epididymal Spam1 (PH- 20) Is Released in the Luminal Fluid With its Lipid Anchor. *J. Androl.* **24,** 51–58 (2003).

11. Kaneiwa, T., Mizumoto, S., Sugahara, K. & Yamada, S. Identification of human hyaluronidase-4 as a novel chondroitin sulfate hydrolase that preferentially cleaves the galactosaminidic linkage in the trisulfated tetrasaccharide sequence. *Glycobiology* **20,** 300–309 (2010).

12. Hemming, R. *et al.* Mouse Hyal3 encodes a 45- to 56-kDa glycoprotein whose overexpression increases hyaluronidase 1 activity in cultured cells. *Glycobiology* **18,** 280–289 (2008).

13. Zhang, L. *et al.* Hyaluronidase activity of human Hyal1 requires active site acidic and tyrosine residues. *J. Biol. Chem.* **284,** 9433–42 (2009).

14. Reissig, J. L., Strominger, J. L. & Leloir, L. F. A modified colorimetric method for estimation of N-acetylamino sugars*.

15. Frost, G. I. & Stern, R. A microtiter-based assay for hyaluronidase activity not requiring specialized reagents. *Anal. Biochem.* **251,** 263–269 (1997).

16. Guntenhöner, M. W., Pogrel, M. A. & Stern, R. A substrate-gel assay for hyaluronidase activity. *Matrix* **12,** 388–396 (1992).

17. Lepperdinger, G., Strobl, B. & Kreil, G. HYAL2, a human gene expressed in many cells, encodes a lysosomal hyaluronidase with a novel type of specificity. *J. Biol. Chem.* **273,** 22466–70 (1998).

18. Bourguignon, L. Y. W., Singleton, P. A., Diedrich, F., Stern, R. & Gilad, E. CD44 Interaction with Na+-H+ Exchanger (NHE1) Creates Acidic Microenvironments Leading to Hyaluronidase-2 and Cathepsin B Activation and Breast Tumor Cell Invasion. *J. Biol. Chem.* **279,** 26991–27007 (2004).

19. Vigdorovich, V., Strong, R. K. & Miller, A. D. Expression and Characterization of a Soluble, Active Form of the Jaagsiekte Sheep Retrovirus Receptor, Hyal2. *J. Virol.* **79,** 79–86 (2005).

20. Vigdorovich, V., Miller, A. D. & Strong, R. K. Ability of hyaluronidase 2 to degrade extracellular hyaluronan is not required for its function as a receptor for jaagsiekte sheep retrovirus. *J. Virol.* **81,** 3124–9 (2007).

21. Harada, H. & Takahashi, M. CD44-dependent Intracellular and Extracellular Catabolism of Hyaluronic Acid by Hyaluronidase-1 and -2 *. (2006). doi:10.1074/jbc.M608358200

22. Shuttleworth, T. L., Wilson, M. D., Wicklow, B. A., Wilkins, J. A. & Triggs-Raine, B. L. Characterization of the murine hyaluronidase gene region reveals complex organization and cotranscription of Hyal1 with downstream genes, Fus2 and Hyal3. *J. Biol. Chem.* **277,** 23008–18 (2002).

23. Puissant, E. *et al.* Subcellular trafficking and activity of hyal-1 and its processed forms in murine macrophages. *Traffic* **15,** 500–515 (2014).

24. Gasingirwa, M.-C. *et al.* Endocytosis of hyaluronidase-1 by the liver. *Biochem. J.* **430,** 305–313 (2010).

25. Chao, K. L., Muthukumar, L. & Herzberg, O. Structure of human hyaluronidase-1, a hyaluronan hydrolyzing enzyme involved in tumor growth and angiogenesis. *Biochemistry* **46,** 6911–20 (2007).

26. Triggs-Raine, B., Salo, T. J., Zhang, H., Wicklow, B. a & Natowicz, M. R. Mutations in HYAL1, a member of a tandemly distributed multigene family encoding disparate hyaluronidase activities, cause a newly described lysosomal disorder, mucopolysaccharidosis IX. *Proc. Natl. Acad. Sci. U. S. A.* **96,** 6296–6300 (1999).

27. Martin, D. C. *et al.* A mouse model of human mucopolysaccharidosis IX exhibits osteoarthritis. *Hum. Mol. Genet.* **17,** 1904–1915 (2008).

28. Strobl, B., Wechselberger, C., Beier, D. R. & Lepperdinger, G. Structural organization and chromosomal localization of Hyal2, a gene encoding a lysosomal hyaluronidase. *Genomics* **53,** 214–219 (1998).

29. Rai, S. K. *et al.* Candidate Tumor Suppressor HYAL2 is a Glycosylphosphatidylinositol (GPI)-Anchored Cell-Surface Receptor for Jaagsiekte Sheep Retrovirus, the Envelope

Protein of Which Mediates Oncogenic Transformation. *Proceedings of the National Academy of Sciences of the United States of America* **98,** 4443–4448

30. Andre, B. *et al.* Hyal2 is a glycosylphosphatidylinositol-anchored, lipid raft-associated hyaluronidase. *Biochem. Biophys. Res. Commun.* **411,** 175–179 (2011).

31. Marei, W. F. A., Salavati, M. & Fouladi-Nashta, A. A. Critical role of hyaluronidase-2 during preimplantation embryo development. *Mol. Hum. Reprod.* **19,** 590–599 (2013).

32. Chowdhury, B., Hemming, R., Faiyaz, S. & Triggs-Raine, B. Hyaluronidase 2 (HYAL2) is expressed in endothelial cells, as well as some specialized epithelial cells, and is required for normal hyaluronan catabolism. *Histochem. Cell Biol.* **145,** 53–66 (2016).

33. Miller, A. D. *et al.* Hyal2, where are you? *Osteoarthr. Cartil.* **14,** 1315–7 (2006).

34. Lepperdinger, G., Müllegger, J. & Kreil, G. Hyal2 - Less active, but more versatile? *Matrix Biology* **20,** 509–514 (2001).

35. Bourguignon, V. & Flamion, B. Respective roles of hyaluronidases 1 and 2 in endogenous hyaluronan turnover. *FASEB J.* **30,** 2108–14 (2016).

36. Chow, G., Knudson, C. B. & Knudson, W. Expression and cellular localization of human hyaluronidase-2 in articular chondrocytes and cultured cell lines. *Osteoarthr. Cartil.* **14,** 849–858 (2006).

37. Duterme, C., Mertens-Strijthagen, J., Tammi, M. & Flamion, B. Two novel functions of hyaluronidase-2 (Hyal2) are formation of the glycocalyx and control of CD44-ERM interactions. *J. Biol. Chem.* **284,** 33495–33508 (2009).

38. Chang, N.-S. Transforming growth factor-beta1 blocks the enhancement of tumor necrosis factor cytotoxicity by hyaluronidase Hyal-2 in L929 fibroblasts. *BMC Cell Biol.* **3,** 8 (2002).

39. Hsu, L.-J. *et al.* Transforming Growth Factor β1 Signaling via Interaction with Cell Surface Hyal-2 and Recruitment of WWOX/WOX1. *J. Biol. Chem.* **284,** 16049–16059 (2009).

40. de la Motte, C. *et al.* Platelet-derived hyaluronidase 2 cleaves hyaluronan into fragments that trigger monocyte-mediated production of proinflammatory cytokines. *Am. J. Pathol.* **174,** 2254–2264 (2009).

41. Jadin, L. *et al.* Skeletal and hematological anomalies in HYAL2-deficient mice: a second type of mucopolysaccharidosis IX? *FASEB J.* **22,** 4316–4326 (2008).

42. Chowdhury, B., Hemming, R., Hombach-Klonisch, S., Flamion, B. & Triggs-Raine, B. Murine hyaluronidase 2 deficiency results in extracellular hyaluronan accumulation and severe cardiopulmonary dysfunction. *J. Biol. Chem.* **288,** 520–528 (2013).

43. Chowdhury, B., Xiang, B., Muggenthaler, M., Dolinsky, V. W. & Triggs-Raine, B. Hyaluronidase 2 deficiency is a molecular cause of cor triatriatum sinister in mice. *Int. J. Cardiol.* **209,** 281–283 (2016).

44. Muggenthaler, M. M. A. *et al.* Mutations in HYAL2, Encoding Hyaluronidase 2, Cause a

Syndrome of Orofacial Clefting and Cor Triatriatum Sinister in Humans and Mice. *PLoS Genet.* **13,** (2017).

45. Meyer, K. & Palmer, J. W. The polysaccharide of the vitreous humor.

46. Balazs, E. A., Laurent, T. C. & Jeanloz, R. W. Nomenclature of hyaluronic acid. *Biochem. J.* **235,** (1986).

47. Stern, R., Asari, A. A. & Sugahara, K. N. Hyaluronan fragments: An information-rich system. *Eur. J. Cell Biol.* **85,** 699–715 (2006).

48. Laurent, T. C., Laurent, U. B. & Fraser, J. R. E. The structure and function of hyaluronan: An overview. *Immunol. Cell Biol.* **74,** A1–A7 (1996).

49. Fraser, J. R. & Laurent, T. C. Turnover and metabolism of hyaluronan. *Ciba Found Symp* **143,** 41-49-285 (1989).

50. Laurent, C., Johnson-Wells, G., Hellström, S., Engström-Laurent, A. & Wells, A. F. Localization of hyaluronan in various muscular tissues. *Cell Tissue Res.* **263,** 201–205 (1991).

51. Reed, R. K., Lija, K. & Laurent, T. C. Hyaluronan in the rat with special reference to the skin. *Acta Physiol. Scand.* **134,** 405–411 (1988).

52. Fraser, J. R., Laurent, T. C. & Laurent, U. B. Hyaluronan: its nature, distribution, functions and turnover. *J. Intern. Med.* **242,** 27–33 (1997).

53. Fenderson, B. A., Stamenkovic, I. & Aruffo, A. Localization of hyaluronan in mouse embryos during implantation, gastrulation and organogenesis. *Differentiation.* **54,** 85–98 (1993).

54. Evanko, S. P. & Wight, T. N. Intracellular Localization of Hyaluronan in Proliferating Cells. *J. Histochem. Cytochem.* **47,** 1331–1341 (1999).

55. Prehm, P. Synthesis of hyaluronate in differentiated teratocarcinoma cells. Mechanism of chain growth. *Biochem. J.* **211,** 191–198 (1983).

56. Weigel, P. H., Hascall, V. C. & Tammi, M. Hyaluronan synthases. *J. Biol. Chem.* **272,** 13997–4000 (1997).

57. Ouskova, G., Spellerberg, B. & Prehm, P. Hyaluronan release from Streptococcus pyogenes: Export by an ABC transporter. *Glycobiology* **14,** 931–938 (2004).

58. Schulz, T., Schumacher, U. & Prehm, P. Hyaluronan export by the ABC transporter MRP5 and its modulation by intracellular cGMP. *J. Biol. Chem.* **282,** 20999–21004 (2007).

59. Weigel, P. H. Hyaluronan Synthase: The Mechanism of Initiation at the Reducing End and a Pendulum Model for Polysaccharide Translocation to the Cell Exterior. *International Journal of Cell Biology* **2015,** (2015).

60. Itano, N. *et al.* Three isoforms of mammalian hyaluronan synthases have distinct enzymatic properties. *J. Biol. Chem.* **274,** 25085–92 (1999).

61.   Törrönen, K. *et al.* Tissue distribution and subcellular localization of hyaluronan synthase isoenzymes. *Histochem. Cell Biol.* **141,** 17–31 (2014).

62.   Camenisch, T. D. *et al.* Disruption of hyaluronan synthase-2 abrogates normal cardiac morphogenesis and hyaluronan-mediated transformation of epithelium to mesenchyme. *J. Clin. Invest.* **106,** 349–360 (2000).

63.   Bai, K. J. *et al.* The role of hyaluronan synthase 3 in ventilator-induced lung injury. *Am. J. Respir. Crit. Care Med.* **172,** 92–98 (2005).

64.   Mack, J. A. *et al.* Enhanced Inflammation and Accelerated Wound Closure Following Tetraphorbol Ester Application or Full-Thickness Wounding in Mice Lacking Hyaluronan Synthases Has1 and Has3. *J. Invest. Dermatol.* **132,** 198–207 (2012).

65.   Tien, J. Y. L. & Spicer, A. P. Three vertebrate hyaluronan synthases are expressed during mouse development in distinct spatial and temporal patterns. *Dev. Dyn.* **233,** 130–141 (2005).

66.   Kobayashi, N. *et al.* Hyaluronan Deficiency in Tumor Stroma Impairs Macrophage Trafficking and Tumor Neovascularization. *Cancer Res.* **70,** 7073–7083 (2010).

67.   Arranz, A. M. *et al.* Hyaluronan Deficiency Due to Has3 Knock-Out Causes Altered Neuronal Activity and Seizures via Reduction in Brain Extracellular Space. *J. Neurosci.* **34,** 6164–6176 (2014).

68.   Adamia, S. *et al.* Inherited and acquired variations in the hyaluronan synthase 1 (HAS1) gene may contribute to disease progression in multiple myeloma and Waldenstrom macroglobulinemia. *Blood* **112,** 5111–5121 (2008).

69.   Kuppusamy, H. *et al.* Inherited Polymorphisms in Hyaluronan Synthase 1 Predict Risk of Systemic B-Cell Malignancies but Not of Breast Cancer. *PLoS One* **9,** e100691 (2014).

70.   Spicer, A. P., Tien, J. L., Joo, A. & Bowling, Jr, R. A. Investigation of hyaluronan function in the mouse through targeted mutagenesis. *Glycoconj. J.* **19,** 341–345 (2002).

71.   Camenisch, T. D., Schroeder, J. A., Bradley, J., Klewer, S. E. & McDonald, J. A. Heart-valve mesenchyme formation is dependent on hyaluronan-augmented activation of ErbB2-ErbB3 receptors. *Nat. Med.* **8,** (2002).

72.   Matsumoto, K. *et al.* Conditional inactivation of Has2 reveals a crucial role for hyaluronan in skeletal growth, patterning, chondrocyte maturation and joint formation in the developing limb. *Development* **136,** 2825–2835 (2009).

73.   Schiller, S., Mathews, M. B., Goldfaber, L., Ludowieg, J. & Dorfman, A. The metabolism of mucopolysaccharies in animals II. Studies in skin utilizing labeled acetate*.

74.   Schiller, S. *et al.* The metabolism of mucopolysaccharides in animals III. Further studies of skin utlizing C14-Glucose, C14-acetate, and S36-sodium sulfate*.

75.   Laurent, T. C., Laurent, U. B. G. & Fraser, J. R. E. Serum hyaluronan as a disease marker. *Ann. Med.* **28,** 241–253 (1996).

76.   Fraser, J. R., Laurent, T. C., Pertoft, H. & Baxter, E. Plasma clearance, tissue distribution

and metabolism of hyaluronic acid injected intravenously in the rabbit. *Biochem. J.* **200,** 415–24 (1981).

77. Fraser, J. R., Laurent, T. C., Engstrom-Laurent, A. & Laurent, U. G. Elimination of hyaluronic acid from the blood stream in the human. *Clin Exp Pharmacol Physiol* **11,** 17–25 (1984).

78. Laurent, T. C. *et al.* Urinary excretion of hyaluronan in man. *Scand. J. Clin. Lab. Invest.* **47,** 793–799 (1987).

79. Fraser, J. R. E., Appelgren, L. E. & Laurent, T. C. Tissue uptake of circulating hyaluronic acid - A whole body autoradiographic study. *Cell Tissue Res.* **233,** 285–293 (1983).

80. Gushulak, L. *et al.* Hyaluronidase 1 and ??-hexosaminidase have redundant functions in hyaluronan and chondroitin sulfate degradation. *J. Biol. Chem.* **287,** 16689–16697 (2012).

81. Linker, A., Meyer, K. & Weissmanns, B. Enzymatic formation of monosaccharides from hyaluronate*.

82. Fenderson, B. A., Stamenkovic, I. & Aruffo, A. Localization of hyaluronan in mouse embryos during implantation, gastrulation and organogenesis. *Differentiation* **54,** 85–98 (1993).

83. Brown, J. J. & Papaioannou, V. E. Ontogeny of hyaluronan secretion during early mouse development. *Development* **117,** 483–492 (1993).

84. Toole, B. P. Hyaluronan in morphogenesis. *Semin. Cell Dev. Biol.* **12,** 79–87 (2001).

85. Day, A. J. & Prestwich, G. D. Hyaluronan-binding Proteins: Tying Up the Giant*. (2001).

86. Kultti, A. *et al.* Hyaluronan Synthesis Induces Microvillus-like Cell Surface Protrusions *S. (2006).

87. Turley, E. A., Roth, S. & Hakomori, S. Spontaneous glycosylation of glycosaminoglycan substrates by adherent fibroblasts. *Cell* **17,** 109–15 (1979).

88. Turley, E. A., Bowman, P. & Kytryk, M. A. Effects of hyaluronate and hyaluronate binding proteins on cell motile and contact behaviour. *J. Cell Sci* **78,** 133–145 (1985).

89. Turley, E. A., Austen, L., Vandeligt, K. & Clary, C. Hyaluronan and a Cell-associated Hyaluronan Binding Protein Regulate the Locomotion of Ras-transformed Cells.

90. Ruoslahti, E. & Yamaguchi, Y. Proteoglycans as modulators of growth factor activities. *Cell* **64,** 867–869 (1991).

91. Nieto, M. A. The early steps of neural crest development. *Mech. Dev.* **105,** 27–35 (2001).

92. Zoltan-Jones, A., Huang, L., Ghatak, S. & Toole, B. P. Elevated Hyaluronan Production Induces Mesenchymal and Transformed Properties in Epithelial Cells. *J. Biol. Chem.* **278,** 45801–45810 (2003).

93. Shukla, S. *et al.* Synthesis and Organization of Hyaluronan and Versican by Embryonic Stem Cells Undergoing Embryoid Body Differentiation. *J. Histochem. Cytochem.* **58,** 345–358 (2010).

94. Kosaki, R., Watanabe, K. & Yamaguchi, Y. Overproduction of hyaluronan by expression of the hyaluronan synthase Has2 enhances anchorage-independent growth and tumorigenicity. *Cancer Res.* **59,** 1141–1145 (1999).

95. Kultti, A. *et al.* Accumulation of Extracellular Hyaluronan by Hyaluronan Synthase 3 Promotes Tumor Growth and Modulates the Pancreatic Cancer Microenvironment. *Biomed Res. Int.* **2014,** (2014).

96. Markwald, R. R., Fitzharris, T. P., Bank, H. & Bernanke, D. H. Structural analyses on the matrical organization of glycosaminoglycans in developing endocardial cushions. *Dev. Biol.* **62,** (1978).

97. Morris-Wiman, J. & Brinkley, L. An extracellular matrix infrastructure provides support for murine secondary palatal shelf remodelling. *Anat. Rec.* **234,** (1992).

98. Weston, J. A., Pintar, J. E., Derby, M. A. & Nichols, D. H. The morphogenesis of spinal ganglia from neural crest cells. *Prog. Clin. Biol. Res.* **15,** (1977).

99. Toole, B. P. & Gross, J. The extracellular matrix of the regenerating newt limb: Synthesis and removal of hyaluronate prior to differentiation. *Dev. Biol.* **25,** 57–77 (1971).

100. Nandadasa, S., Foulcer, S. & Apte, S. S. The multiple, complex roles of versican and its proteolytic turnover by ADAMTS proteases during embryogenesis. *Matrix Biol.* **35,** 34–41 (2014).

101. Pohl, M., Sakurai, H., Stuart, R. O. & Nigam, S. K. Role of Hyaluronan and CD44 in in Vitro Branching Morphogenesis of Ureteric Bud Cells.

102. Gakunga, P. *et al.* Hyaluronan is a prerequisite for ductal branching morphogenesis. *Development* **124,** 3987–97 (1997).

103. Toole, B., Banerjee, S., Turner, R., Munaim, S. & Knudson, C. in *Developmental Patterning of the Vertebrate Limb* 215–223 (Springer US, 1991). doi:10.1007/978-1-4615-3310-8_30

104. Maleski, M. P. & Knudson, C. B. Hyaluronan-Mediated Aggregation of Limb Bud Mesenchyme and Mesenchymal Condensation during Chondrogenesis. *Exp. Cell Res.* **225,** 55–66 (1996).

105. Underhill, C. B. Hyaluronan is inversely correlated with the expression of CD44 in the dermal condensation of the embryonic hair follicle. *J Invest Dermatol* **101,** 0–820 (1993).

106. Chowdhury, B. *et al.* Hyaluronidase 2 Deficiency Causes Increased Mesenchymal Cells, Congenital Heart Defects, and Heart Failure. *Circ. Cardiovasc. Genet.* **10,** (2017).

107. Taneyhill, L. A. & Bronner-Fraser, M. Recycling signals in the neural crest. *J Biol* **4,** 10 (2005).

108. Etchevers, H. C., Amiel, J. & Lyonnet, S. Molecular bases of human neurocristopathies. *Advances in Experimental Medicine and Biology* **589,** 213–234 (2006).

109. Solis, M. A. *et al.* Hyaluronan Regulates Cell Behavior: A Potential Niche Matrix for Stem Cells. *Biochem. Res. Int.* **2012,** 1–11 (2012).

110. Matrosova, V. Y., Orlovskaya, I. a, Serobyan, N. & Khaldoyanidi, S. K. Hyaluronic acid facilitates the recovery of hematopoiesis following 5-fluorouracil administration. *Stem Cells* **22,** 544–55 (2004).

111. Ferguson, M. W. Palate development. *Development* **103 Suppl,** 41–60 (1988).

112. Gritli-Linde, A. Molecular control of secondary palate development. *Dev. Biol.* **301,** 309–326 (2007).

113. Pratt, R. M., Goggins, J. F., Wilk, A. L. & King, C. T. Acid mucopolysaccharide synthesis in the secondary palate of the developing rat at the time of rotation and fusion. *Dev. Biol.* **32,** 230–7 (1973).

114. Casini, P., Nardi, I. & Ori, M. Hyaluronan is required for cranial neural crest cells migration and craniofacial development. *Dev. Dyn.* **241,** 294–302 (2012).

115. Chai, Y. & Maxson, R. E. Recent advances in craniofacial morphogenesis. *Dev. Dyn.* **235,** 2353–2375 (2006).

116. Cordero, D. R. *et al.* Cranial neural crest cells on the move: Their roles in craniofacial development. *Am. J. Med. Genet. Part A* **155,** 270–279 (2011).

117. Kalluri, R. & Weinberg, R. a. Review series The basics of epithelial-mesenchymal transition. *J. Clin. Invest.* **119,** 1420–1428 (2009).

118. Couly, G., Creuzet, S., Bennaceur, S., Vincent, C. & Le Douarin, N. M. Interactions between Hox-negative cephalic neural crest cells and the foregut endoderm in patterning the facial skeleton in the vertebrate head. *Development* **129,** 1061–73 (2002).

119. Hu, D. & Helms, J. A. The role of Sonic hedgehog in normal and abnormal craniofacial morphogenesis. *Development* **126,** (1999).

120. Helms, J. A., Cordero, D. & Tapadia, M. D. New insights into craniofacial morphogenesis. *Development* **132,** 851–861 (2005).

121. Matthews, J. L. K., Oddone-Paolucci, E. & Harrop, R. A. The Epidemiology of Cleft Lip and Palate in Canada, 1998 to 2007. *Cleft Palate-Craniofacial J.* **52,** 417–424 (2015).

122. Murray, J. C. & Schutte, B. C. Cleft palate: players, pathways, and pursuits. *J. Clin. Invest.* **113,** 1676–1678 (2004).

123. Stanier, P. & Moore, G. E. Genetics of cleft lip and palate: syndromic genes contribute to the incidence of non-syndromic clefts. *Hum. Mol. Genet.* **13,** 73R–81 (2004).

124. Wyszynski, D. F. *Cleft lip and palate : from origin to treatment.* (Oxford University Press, 2002).

125. Tolarova, M. I. A study of the incidence, sex-ratio, laterality and clinical severity in 3,660 probands with facial clefts in Czechoslovakia. *Acta Chir. Plast.* **29,** (1987).

126. Amberger, J. S. & Hamosh, A. Searching online mendelian inheritance in man (OMIM): A knowledgebase of human genes and genetic phenotypes. *Curr. Protoc. Bioinforma.* **2017,** 1.2.1-1.2.12 (2017).

127. Braybrook, C. *et al.* Craniofacial expression of human and murine TBX22 correlates with the cleft palate and ankyloglossia phenotype observed in CPX patients. *Hum. Mol. Genet.* **11,** 2793–2804 (2002).

128. Murray, J. C. *et al.* Linkage of an autosomal dominant clefting syndrome (Van der Woude) to loci on chromosome Iq. *Am. J. Hum. Genet.* **46,** 486–91 (1990).

129. Brunner, H. G., Hamel, B. C. J. & Bokhoven, H. van. P63 gene mutations and human developmental syndromes. *Am. J. Med. Genet.* **112,** 284–290 (2002).

130. O'Brien, K. E., Shorrock, J. & Bianchi, D. W. Prenatal diagnosis of acro-dermatoungual-lacrimal-tooth syndrome, a dominantly inherited ectrodactyly. *J. Ultrasound Med.* **21,** 921–925 (2002).

131. Rodgers, L. S. *et al.* Depolymerized hyaluronan induces vascular endothelial growth factor, a negative regulator of developmental epithelial-to-mesenchymal transformation. *Circ. Res.* **99,** 583–589 (2006).

132. Singh, G. D., Moxham, B. J., Langley, M. S., Waddington, R. J. & Embery, G. Changes in the composition of glycosaminoglycans during normal palatogenesis in the rat. *Arch. Oral Biol.* **39,** 401–407 (1994).

133. Pilloni A, B. G. Low molecular weight hyaluronic acid increases osteogenesis in vitro. *J. Dent. Res.* **71,** 574 (1992).

134. Altschul, S. F., Gish, W., Miller, W., Myers, E. W. & Lipman, D. J. Basic local alignment search tool. *J. Mol. Biol.* **215,** 403–410 (1990).

135. Zhang, Y. I-TASSER server for protein 3D structure prediction. *BMC Bioinformatics* **9,** 40 (2008).

136. Marković-Housley, Z. *et al.* Crystal structure of hyaluronidase, a major allergen of bee venom. *Structure* **8,** 1025–1035 (2000).

137. Davies, G. J., Planas, A. & Rovira, C. Conformational analyses of the reaction coordinate of glycosidases. *Acc. Chem. Res.* **45,** 308–316 (2012).

138. Tews, I. *et al.* Bacterial chitobiase structure provides insight into catalytic mechanism and the basis of Tay-Sachs disease. *Nature structural biology* **3,** 638–48 (1996).

139. DeLano, W. L. The PyMOL Molecular Graphics System. *Schrödinger LLC wwwpymolorg* **Version 1.,** http://www.pymol.org (2002).

140. Natowicz, M. R. & Wang, Y. Human serum hyaluronidase: Characterization of a clinical assay. *Clin. Chim. Acta* **245,** 1–6 (1996).

141. Yoshiki, S., Umeda, T. & Kurahashi, Y. An effective reactivation of alkaline phosphatase in hard tissues completely decalcified for light and electron microscopy. *Histochemie* **29,** 296–304 (1972).

142. Thompson, J. D., Gibson, T. J. & Higgins, D. G. Multiple sequence alignment using ClustalW and ClustalX. *Curr. Protoc. Bioinformatics* **Chapter 2,** Unit 2.3 (2002).

143. Felsenstein, J. PHYLIP - Phylogeny Inference Package, Version 3.69. (Seattle, WA: University of Washington). *Am. Nat.* **171,** 713–725 (2009).

144. Atmuri, V. *et al.* Hyaluronidase 3 (HYAL3) knockout mice do not display evidence of hyaluronan accumulation. *Matrix Biol.* **27,** 653–660 (2008).

145. Nakashima, K. & De Crombrugghe, B. Transcriptional mechanisms in osteoblast differentiation and bone formation. *Trends in Genetics* **19,** 458–466 (2003).

146. Golub, E. E. & Boesze-Battaglia, K. The role of alkaline phosphatase in mineralization. *Curr. Opin. Orthop.* **18,** 444–448 (2007).

147. Oka, K. *et al.* Roles of Collagen and Periostin Expression by Cranial Neural Crest Cells during Soft Palate Development. *J. Histochem. Cytochem.* **60,** 57–68 (2012).

148. Cobo, T. *et al.* Role of periostin in adhesion and migration of bone remodeling cells. *PLoS One* **11,** (2016).

149. Oshima, A. *et al.* A novel mechanism for the regulation of osteoblast differentiation: Transcription of periostin, a member of the fasciclin I family, is regulated by the bHLH transcription factor, twist. *J. Cell. Biochem.* **86,** 792–804 (2002).

150. Camenisch, T. D. *et al.* Disruption of hyaluronan synthase-2 abrogates normal cardiac morphogenesis and hyaluronan-mediated transformation of epithelium to mesenchyme. *J. Clin. Invest.* **106,** 349–360 (2000).

151. Pauws, E. *et al.* Tbx22null mice have a submucous cleft palate due to reduced palatal bone formation and also display ankyloglossia and choanal atresia phenotypes. *Hum. Mol. Genet.* **18,** 4171–4179 (2009).

152. Boskey, A. L., Maresca, M., Wikstrom, B. & Hjerpe, A. Hydroxyapatite formation in the presence of proteoglycans of reduced sulfate content: Studies in the brachymorphic mouse. *Calcif. Tissue Int.* **49,** 389–393 (1991).

153. Shamblott, M. J., Bugg, E. M., Lawler, A. M. & Gearhart, J. D. Craniofacial abnormalities resulting from targeted disruption of the murine Sim2 gene. *Dev. Dyn.* **224,** 373–380 (2002).

154. Goudy, S., Law, A., Sanchez, G., Baldwin, H. S. & Brown, C. Tbx1 is necessary for palatal elongation and elevation. *Mech. Dev.* **127,** 292–300 (2010).

155. Zhao, N., Wang, X., Qin, L., Guo, Z. & Li, D. Effect of molecular weight and concentration of hyaluronan on cell proliferation and osteogenic differentiation in vitro. *Biochem. Biophys. Res. Commun.* **465,** 569–574 (2015).

156. Pilloni, A. & Bernard, G. W. The effect of hyaluronan on mouse intramembranous osteogenesis in vitro. *Cell Tissue Res.* **294,** 323–333 (1998).

157. Wegner, M. Secrets to a healthy Sox life: Lessons for melanocytes. *Pigment Cell Research* **18,** 74–85 (2005).

158. Pingault, V. *et al.* Loss-of-function mutations in SOX10 cause Kallmann syndrome with deafness. *Am. J. Hum. Genet.* **92,** 707–724 (2013).

159. Suzuki, E. *et al.* Loss-of-function SOX10 mutation in a patient with kallmann syndrome, hearing loss, and iris hypopigmentation. *Horm. Res. Paediatr.* **84,** 212–216 (2015).

160. Gibson, T. J., Seiler, M. & Veitia, R. A. The transience of transient overexpression. *Nat. Methods* **10,** 715–721 (2013).

161. Moriya, H. Quantitative nature of overexpression experiments. *Mol. Biol. Cell* **26,** 3932–3939 (2015).

162. Potter, A. S. & Potter, S. S. Molecular anatomy of palate development. *PLoS One* **10,** (2015).